Title: Fluid-related inclusions in Alpine high-pressure peridotite reveal trace element recycling during subduction-zone dehydration of serpentinized mantle (Cima di Gagnone, Swiss Alps)

Abstract: The garnet metaperidotite and chlorite harzburgite bodies embedded in paragneisses in the tectonic mélange delineating the subduction interface at Cima di Gagnone are unique examples of ultramafic rocks that experienced multistage subduction metasomatism and devolatilization. Eclogite-facies olivine and garnet of garnet metaperidotite and chlorite harzburgite trap primary to pseudosecondary polyphase inclusions recording the fluid evolved during breakdown of antigorite and chlorite. Combined major element mapping and laser-ablation ICP-MS bulk inclusion analysis characterize the mineral composition of the polyphase inclusions and quantify the fluid chemistry. Silicates, Cl-bearing phases, sulfides, carbonates, and oxides document post-entrapment mineral growth starting immediately after fluid entrapment.

Compositional data reveal the presence of two different fluid types. The first type is hosted in olivine of the garnet metaperidotite and shows pronounced fluid-mobile and light rare earth element enrichments, with up to 103 PM (primitive mantle) Cl, Cs, Pb, As, Sb, ~102 PM Tl, Ba, while Rb, B, Sr, Li, U are of the order of 101 PM, and alkalis are ~2 PM. The second fluid type hosted by garnet and by olivine of the chlorite harzburgite is much less enriched in fluid-mobile elements but shows overall similar enrichment patterns. These data reveal a multistage fluid history affecting these peridotite lenses, including selective element enrichment during seafloor alteration followed by fluid rock interaction during subduction metamorphism along the plate interface. Here, sediment-equilibrated fluid infiltration produced serpentinized metaperidotites strongly enriched in fluid-mobile elements that were released again at greater depth upon dehydration. The fluid inclusions hosted by garnet may then record the composition of the chlorite breakdown fluid.

These data demonstrate that hydrous ultrabasic rocks may act as a sink and transporter of water and fluid-mobile element enrichments generated by both ocean floor hydration and fluid-mobile element enrichment via sediment equilibrated fluids during early subduction stages. Consequently, serpentinite devolatilization at subarc depths produces fluids enriched in crust and sediment-derived components to flux-melt the mantle wedge triggering arc magmatism, without the need of concomitant dehydration/melting of metasedimentary or altered oceanic crust lithologies.

1   **Fluid-related inclusions in Alpine high-pressure peridotite reveal trace element**

2   **recycling during subduction-zone dehydration of serpentinized mantle (Cima di**

3   **Gagnone, Swiss Alps)**

4

5   [1*]Marco Scambelluri, [2]Thomas Pettke, [1]Enrico Cannaò

6

7   [1]Dipartimento di Scienze della Terra, Ambiente e Vita, Università di Genova, Italy

8   [2] Institute of Geological Sciences, University of Bern, Switzerland

9   * Corresponding author: marco.scambelluri@dipteris.unige.it

10

13

16

Abstract

17

18   The garnet metaperidotite and chlorite harzburgite bodies embedded in paragneisses in the
     tectonic mélange delineating the subduction interface at Cima di Gagnone are unique

19   examples of ultramafic rocks that experienced multistage subduction metasomatism and

20   devolatilization. Eclogite-facies olivine and garnet of garnet metaperidotite and chlorite

21   harzburgite trap primary to pseudosecondary polyphase inclusions recording the fluid

22   evolved during breakdown of antigorite and chlorite. Combined major element mapping and laser-

23   ablation ICP-MS bulk inclusion analysis characterize the mineral composition of the polyphase

24   inclusions and quantify the fluid chemistry. Silicates, Cl-bearing phases, sulfides, carbonates, and

25   oxides document post-entrapment mineral growth starting immediately after

26 fluid entrapment.

27   Compositional data reveal the presence of two different fluid types. The first type is

28 hosted in olivine of the garnet metaperidotite and shows pronounced fluid-mobile and light

29 rare earth element enrichments, with up to 10^3 PM (primitive mantle) Cl, Cs, Pb, As, Sb, $\sim 10^2$

30 PM Tl, Ba, while Rb, B, Sr, Li, U are of the order of 10^1 PM, and alkalis are ~ 2 PM. The second

31 fluid type hosted by garnet and by olivine of the chlorite harzburgite is much less enriched in

32 fluid-mobile elements but shows overall similar enrichment patterns. These data reveal a

33 multistage fluid history affecting these peridotite lenses, including selective element

34 enrichment during seafloor alteration followed by fluid rock interaction during subduction

35 metamorphism along the plate interface. Here, sediment-equilibrated fluid infiltration

36 produced serpentinized metaperidotites strongly enriched in fluid-mobile elements that were

37 released again at greater depth upon dehydration. The fluid inclusions hosted by garnet may

38 then record the composition of the chlorite breakdown fluid.

39   These data demonstrate that hydrous ultrabasic rocks may act as a sink and transporter

40 of water and fluid-mobile element enrichments generated by both ocean floor hydration and

41 fluid-mobile element enrichment via sediment equilibrated fluids during early subduction

42 stages. Consequently, serpentinite devolatilization at subarc depths produces fluids enriched

43 in crust and sediment-derived components to flux-melt the mantle wedge triggering arc

44 magmatism, without the need of concomitant dehydration/melting of metasedimentary or

45 altered oceanic crust lithologies.

46

47

48 **1. Introduction**

49 Serpentinites trigger major tectonic and geochemical processes in Earth. Their abundance in

50 oceanic plates and in subduction zones controls the water budgets and properties of slabs and

overlying mantle (Ulmer and Trommsdorff, 1995; Cannat et al., 1995; Iwamori, 1998; Rüpke et al., 2004; Frueh Green et al., 2004). Great importance is now given to the interface domains between subducting and overlying plates, where serpentinite forms kilometre-thick layers derived from hydration of supra-subduction mantle, or occurs in tectonic mélanges atop the slab, as matrix and as blocks of variable size and provenance (Bostock et al., 2002; Federico et al., 2007; Bebout, 2007). In such environments, the low viscosity and high water content of serpentinite control deformation focussing, fluid release and mass transfer (Gerya et al., 2003; Hyndman and Peacock, 2003; Bebout, 2007; Blanco-Quintero et al., 2011; Scambelluri et al., 2014). Several authors proposed that transfer of trace element-rich fluids from slab to mantle is dictated by serpentinite stability and by its capacity of storing water, carbon and fluid-mobile elements (Hattori and Guillot, 2003; Scambelluri et al., 2004a; Sharp and Barnes, 2004; Deschamps et al., 2010; 2011; 2013; Kendrick et al., 2011, 2013; John et al., 2011; Alt et al., 2013; Boschi et al., 2013; Shimizu et al., 2013; Evans et al., 2014; De Hoog et al., 2014). These elements are progressively extracted from serpentinite during the prograde dehydration reactions (1) antigorite + brucite = olivine + fluid, and (2) antigorite = olivine + orthopyroxene + fluid. Reaction (1) occurred in most eclogite-facies Alpine serpentinites, showing antigorite + olivine-bearing parageneses in rocks and in veins draining the released fluid (Plumper et al., 2014). The fluid is Cl-rich and contains variable amounts of B, Li (Scambelluri et al., 1997; 2004a; Scambelluri and Tonarini, 2012). A larger fluid amount is released by reaction (2), experimentally reproduced from ca. 60 km to subarc depth conditions (Ulmer and Trommsdorff, 1995, 1999; Wunder and Schreyer, 1997). Additional fluid is released by chlorite breakdown, leading to formation of garnet-bearing assemblages (Fumagalli and Poli, 2005; Dvir et al., 2011): no constraints yet exist on the composition of the chlorite-dehydration fluid.

75   Breakdown of serpentinzed mantle via reaction (2) is recorded in two main localities:

76   Cerro del Almirez (Spain), where chlorite harzburgite crops out as discrete rock unit, and

77   Cima di Gagnone (Central Alps), where chlorite harzburgite and garnet metaperidotite blocks

78   are embedded in a sedimentary mélange. At both localities the serpentinized protoliths are

79   either preserved as relict bodies inside the chlorite harzburgite (Almirez; Trommsdorff et al.,

80   1998), or as serpentine inclusions in peak minerals (Gagnone; Scambelluri et al., 2014). The

81   antigorite breakdown fluids were analyzed only in the Almirez rocks: they correspond to

82   polyphase inclusions hosting olivine, magnetite, a hydrous phase and liquid water enriched in

83   B, Li, alkalis, Pb, Sr (Scambelluri et al., 2001; 2004a, b). Comparable fluid compositions were

84   experimentally achieed by dehydration of natural Almirez serpentine (Spandler et al., 2014).

85   Together, these results show that serpentinite dehydration fluids are viable agents for

86   metasomatism of the subarc mantle.

87   Exchange with surrounding sedimentary rocks may lead to serpentinite enrichment in

88   specific tracers like As, Be and Sb (Gagnone), in radiogenic Sr and Pb (Gagnone and Almirez)

89   and in light B isotopes (Cannaò et al., 2013; Angiboust et al., 2014). Element addition in

90   serpentinized rocks occurred during prograde burial in Gagnone (Scambelluri et al., 2014;

91   Cannaò et al., 2013), during peak eclogite-facies dehydration in Almirez (Marchesi et al., 2013;

92   Harvey et al, 2014), or during fluid channeling along shear zones within subducting slabs

93   (Angiboust et al., 2014).

94   Although much work has been done to understand serpentinite behavior in subduction

95   zones, the direct analyses of de-serpentinzation fluids are still few (Scambelluri et al., 2001;

96   2004 a, b; Tenthorey and Hermann, 2004; Spandler et al., 2014). Here we address this issue

97   by analyzing natural fluid-related inclusions hosted in eclogitic garnet and olivine in the

98   Gagnone metaperidotites. Because these rocks record influx of sediment-equilibrated fluid

99   during prograde subduction metamorphism (Scambelluri et al., 2014; Cannaò et al., 2013),

100 they represent proxies of mantle metaperidotite metasomatized by slab fluids, as occurs in

101 mélange (Bebout, 2007) and/or in supra-subduction zone mantle (Hyndman and Peacock,

102 2003; Savov et al., 2005; Scambelluri et al., 2008). We present textural observations together

103 with fluid inclusion analysis, with the aim to quantify the composition of serpentine-

104 breakdown fluids and constrain element recycling during subduction.

105

106 **2. Geologic and petrologic background**

107 The Cima di Gagnone (Adula-Cima Lunga Unit, Central Swiss Alps) garnet metaperidotite and

108 chlorite harzburgite investigated here originate from lenses inside paragneiss sequences. Like

109 other peridotite bodies (Alpe Arami, Duria) they are exposed along a continuous horizon in

110 the southern Adula Unit (Moeckel, 1969; Fumasoli, 1974; Evans & Trommsdorff, 1978;

111 Pfiffner & Tromsdorff, 1998), associated with pelitic, mafic and granitoid rocks referred to the

112 European continental margin involved in Alpine subduction and collision. The Adula Unit is

113 affected by high-pressure metamorphism (Heinrich, 1982; 1986), that is absent in the other

114 Central Alpine Units and pre-dates widespread collision-related Lepontine amphibolite-facies

115 metamorphism (Trommsdorff, 1966). The Adula rock association has been interpreted as a

116 '*lithospheric mélange*' (Trommsdoff, 1990) formed in a *tectonic accretionary channel* (Engi et

117 al., 2001) representative of plate-interface environments (Engi et al., 2001; Scambelluri et al.,

118 2014).

119   At Gagnone, chlorite harzburgite lenses are the most widespread; garnet metaperidotite

120 is much less frequent. The chlorite harzburgite bodies host eclogite and metarodingite. The

121 latter rocks suggest that the ultramafic host was serpentinized before peak eclogite-facies

122 dehydration (Evans and Tromsdorff, 1978). Petrography, thermobarometry and

123 pseudosection modelling of the Gagnone garnet metaperidotite document a peak eclogite-

124 facies paragenesis of olivine, clino- and orthopyroxene, Mg-hornblende and garnet,

5

crystallized at 800-850 °C and maximum 3 GPa (Fig. 1a; Evans and Trommsdorff, 1978;

Pfiffner and Trommsdorff, 1998; Nimis and Trommsdorff, 2001; Fumagalli and Poli, 2005;

Scambelluri et al., 2014). In garnet metaperidotite, garnet grows as peak poikilobastic phase

that encloses inclusions of prograde chlorite and Ca-amphibole (Fig. 1a; Scambelluri et al.,

2014). The peak eclogite-facies paragenesis of chlorite harzburgite consists of olivine,

orthopyroxene, chlorite, fluorine-bearing Ti-clinohumite $\pm$ carbonate (Trommsdorff and

Evans, 1983; Scambelluri et al., 2014). For this rock type, thermodynamic modelling suggest

peak crystallization above 650 °C (the antigorite-out reaction) and below 750-800 °C (the

chlorite-out reaction; Scambelluri et al., 2014); pressure is likely below 3GPa (Fig. 1b).

The major and rare earth element (REE) variability of metaperidotites was mostly

acquired during pre-subduction mantle evolution, during partial melting and reactive melt

flow in the oceanic plate (Scambelluri et al., 2014). The ultramafic suite is also characterized

by fluid-mobile element enrichment. Similarity between the U, Pb, B, Li and Sr concentrations

of the Gagnone metaperidotites (Scambelluri et al., 2014) and present-day oceanic

serpentinites (Kodolanyi et al., 2012) suggests that these elements were partly uptaken

during initial serpentinization by seawater-derived fluids (Scambelluri et al., 2014).

Prominent positive Be, As and Sb anomalies suggest involvement of fluids equilibrated with

crustal (metasedimentary) reservoirs during prograde subduction metamorphism and

metaperidotite entrainment in (meta)sediments (Scambelluri et al., 2014; Fig. 1c). Exchange

with sediment-derived fluids is also suggested by metaperidotite enrichment in radiogenic Sr

and Pb to values approaching the composition of country metasediments (Cannaò et al.,

2013). These specific fluid-mobile element enrichments are detected in all peak eclogitic

minerals, and clearly indicate open system prograde subduction metamorphism preceding

the eclogite-facies dehydration. The B, Li, As and Sb concentrations of peak anhydrous

minerals exceed primitive mantle values, demonstrating the potential of dehydrated

150   serpentinite residues to transfer geochemical anomalies deep into the Earth's mantle.

151

152   **3. Inclusion occurrence and petrography**

153   The inclusions inside the high-pressure minerals of the Gagnone metaperidotites can be

154   grouped as: (1) monophase mineral inclusions; (2) polyphase inclusions, hosting a number of

155   minerals intergrown in regular cavities.

156   The first group represents remnants of the pre-eclogitic mineral parageneses and occurs

157   in all metaperidotites. In garnet metaperidotite, prograde chlorite, amphibole, ortho and

158   clinopyroxene inclusions are overgrown by eclogitic poikiloblastic garnet. This indicates that

159   these rocks, besides antigorite dehydration, record later-stage chlorite breakdown and garnet

160   formation (Fig. 1a). In chlorite harzburgite, inclusions of prograde serpentine are preserved in

161   eclogitic fluorine-Ti-clinohumite. The reader is referred to Scambelluri et al. (2014) for more

162   detailed descriptions and for discussion of implications.

163   Microscopy in reflected light has revealed several opaque phases, corresponding to light-

164   grey chromite, magnetite and yellowish sulfides. The latter occur as single inclusions in

165   minerals, as rims and/or overgrowths on chromite, and as interstitial crystals in-between

166   high-pressure minerals; they frequently consist of intergrown crystals of variable chemical

167   composition. Rock-forming sulfides are more abundant in chlorite harzburgite than in garnet

168   metaperidotite.

169   Polyphase inclusions occurs in garnet and olivine from garnet metaperidotite, and in

170   olivine and orthopyroxene from chlorite harzburgite.

171   *Garnet metaperidotite* contains coarse garnet layers and shows coarse centimetres-sized

172   garnet crystals that may correspond to veins or fluid pockets (Figs. 2a, 2b). The coarse garnet

173   (sample MG160-C1) contains myriads of solid polyphase inclusions whose shapes range from

174   geometrically regular to irregular cavities. In general, they are randomly dispersed in garnet

(Figs. 2c,d,f) and are thus interpreted to represent primary fluid inclusions. Similar polyphase inclusions in garnet also occur along planes that do not intersect the garnet grain-boundaries (Fig. 2e). Therefore these inclusions are interpreted to be pseudosecondary. The polyphase inclusions in olivine close to garnet (MG160-C1) are comparable: they are randomly distributed inside olivine and also aligned along microcracks which do not crosscut the olivine grain-boundaries, like primary and pseudosecondary inclusions, respectively (Fig. 4). The inclusions display opaque phases and transparent, birefringent crystals. The polyphase inclusions exposed at the mineral surface contain solids and yellowish sulfide microcrystals. Scanning electron microscopy of exposed, olivine-hosted inclusions has revealed that between inclusion and olivine host a reaction halo made of new olivine developed during post-entrapment fluid-olivine reaction still in the olivine stability field (Fig. 3a). Olivine microcrystals were also identified inside the inclusions (Fig. 3b).

In *chlorite harzburgite,* the polyphase inclusions are hosted by olivine, less frequently by orthopyroxene, and occur only in coarse undeformed samples (MG304-92-1, MG304-92-2). In such samples, rock-forming magnesite can be part of the high-pressure assemblage (Fig. 3c; MG304-92-2) and is partly replaced by rims of retrograde dolomite. The chlorite harzburgite also shows tiny sulfide grains, occurring as inclusions in rock-forming minerals and as interstitial phases in-between high-pressure minerals (Fig. 3d). As for the garnet metaperidotite, the polyphase inclusions are regular to irregular in shape, are mostly randomly dispersed in the host minerals, range in size from several micrometers (the majority) to several tens of micrometers, and contain opaque crystals together with transparent, birefringent phases (Fig. 3e); they rarely follow pseudosecondary trails. Scanning electron microscopy shows the occurrence of olivine (Fig. 3b) and of sulfide microcrystals inside inclusions.

4. Fluid inclusion data reduction

Major element concentrations in inclusion-forming minerals, elemental maps of inclusions, scanning electron microscopy of inclusions, and analysis of the trace element composition of inclusions and hosts were performed by electron microrobe, scanning electron microscopy and laser-ablation-ICP-MS in the Universities of Milano, Genova and Bern. Analytical mehods are described in the repository files.

Data reduction for polyphase inclusion analysis followed the principles developed in Halter et al. (2002). Because an element concentration in the polyphase inclusions cannot independently be determined but is required as the internal standard for data reduction, we adopted the procedures described in detail below. The entire data set is provided in electronic Repository Table R4; inclusion data with consistent patterns are presented here in Table 1.

(1) For garnet-hosted fluid inclusions (sample MG160-C1): Iron shows compatible behavior in the garnet - aqueous fluid system at 4 GPa/800 °C for basaltic bulk composition ($KD_{Fe(fluid-grt)}$ = 0.016; Kessel et al., 2005). Because element distribution coefficients tend to decrease with increasing pressure in aqueous fluid mineral pairs, we employed a $KD_{Fe(fluid-grt)}$ = 0.01 to derive the concentration of FeO = 1.07wt% for the fluid inclusions from the measured garnet FeO = 10.7wt%. We further assumed a total dissolved load of 20wt% for the inclusion fluids, estimated again on the basis of data at 4 GPa/800 °C (Kessel et al., 2005). With this approach, 3 out of 6 high-quality inclusion analyses returned a constant SiO_2 concentration of ca. 10wt%. This SiO_2 concentration was then employed to calculate the element concentrations of the other 3 inclusions, which returned an FeO concentration of ~2.1wt% instead of the inferred 0.17wt%. Note that Fe was calculated exclusively as FeO, lacking constraints on the oxidation state of Fe in the fluid at entrapment. These data suggest that two different types of fluid inclusions were trapped in garnet.

(2) Olivine-hosted inclusions were analyzed for two samples.

225 (2a) For garnet metaperidotite sample MG160-C1, assuming a low Na_2O concentration as

226 above for data reduction did not return results except for two analyses (21frc04; 21frc10). Of

227 these, analysis 21frc04 returned a Na_2O/TiO_2 ratio of 0.08 along with elevated FeO,

228 suggesting accidental entrapment of a Ti-rich mineral (ilmenite?). Therefore, assumed Na2O

229 concentrations of the fluid were incrementally increased for calculation. For Na_2O = 0.5wt%

230 results were obtained for 6 inclusion analyses (21frc06, 21frc08, 21frc09, 21frc11, 21frc12,

231 21frc13). Interestingly, 5 of these show consistent molar Na/Cl ratios of between 0.33 and

232 0.46. Of these, all but inclusion 21frc08 (FeO below detection) returned an FeO concentration

233 of between 1.0 and 1.6wt%. Other two inclusions returned results for an assumed Na_2O =

234 0.1wt%. While their major element pattern is consistent with the inclusions above, their

235 molar Na/Cl ratios are 0.9 and 1.3, respectively and thus clearly different. We therefore use

236 inclusions 21frc09, 21frc11, 21frc12, 21frc13 for further evaluation.

237 (2b) For chlorite harzburgite sample MG304-92-2, a concentration of 0.01wt% Na_2O and

238 10wt% of total dissolved solids was assumed, based on the Na_2O concentration obtained for

239 the garnet-hosted inclusion and the fact that primary inclusions in olivine were likely

240 entrapped at lower P-T than those in garnet (and thus the total dissolved solids are assumed

241 to be lower as argued above). With these constraints, inclusion concentrations could not be

242 calculated for 7 out of 16 inclusions, indicating that they represent mixtures of fluid inclusions

243 and accidentally trapped Cr and Al-bearing Fe-rich spinel. Of the remaining inclusions, that

244 returning an MgO concentration below its limit of detection (analysis 21fra04) and those with

245 an Al_2O3 > 1.5wt% and Cr > 1400µg/g (analyses 21fra12 and 21fra17) were discarded as

246 outliers. Finally, 6 inclusion analyses remained with consistent inclusion element

247 concentrations.

248

249 **5. Mineral content and major element composition of inclusions**

250 Electron microscopy, elemental maps of inclusions, and microprobe analysis of inclusion-

251 forming minerals enabled to identify the main mineral species inside the inclusions. Analyses

252 are reported in Repository Tables R1, R2, R3; the maps of garnet- and of olivine-hosted

253 inclusions are shown in Figures 4 and 5, respectively.

254 *Garnet Metaperidotite.* The maps showing element distribution inside polyphase

255 inclusions in garnet (Fig. 4) reveal the presence of Cl as inclusion component. Chlorine is

256 absent, or below detection in the garnet host. Coincidence in the distribution of Cl, K and Fe

257 suggests the presence of chloride phases. Chlorine is not ubiquitous in garnet-hosted

258 inclusions, because some of them do not reveal detectable amounts of this element (both by

259 SEM and LA-ICP-MS data). Figure 4 also shows the presence of Cr-bearing oxides and of Cu-

260 (and As) bearing sulfides, consistent with the LA-ICP-MS data. In all analyzed inclusions the

261 remaing phases correspond to Ca-amphibole, chlorite and spinel (see Tab. R1). Presence of

262 such mineral infillings in garnet-hosted inclusions is again confirmed by the high Ca and Cr

263 concentrations shown by bulk inclusion analyses (Tab. 1). In some cases, electron microscopy

264 points out that some inclusion minerals can derive from reaction with the host mineral. Ca-

265 amphibole + spinel intergrowths in garnet immediately surrounding the polyphase inclusions

266 can derive from reaction between fluid and host garnet after inclusion entrapment, or may

267 represent the preferred formation of fluid inclusions along with accidentally trapped spinel

268 crystals. While the former poses no limitations to the bulk fluid composition, the latter

269 produces mixtures whose composition is meaningless and therefore discarded from the

270 dataset (analysis 21frc04).

271 Comparable textures affect the olivine-hosted inclusions in garnet metaperidotite (Fig. 5).

272 Olivine from sample MG160-C1 contains inclusions filled with Cr-bearing Fe-oxide, magnetite,

273 Cl-bearing phase and Ni sulfide. The latter differs from sulfide from garnet-hosted inclusions

274 because it lacks Cu and Ni is present as major component (Tab. R3). As a whole, analyses of

the olivine-hosted inclusions yield much more Ni than the garnet-hosted inclusions (Tab. 1), which might be either due to post-entrapment diffusional equilibration between inclusion and host, or to incomplete removal of host olivine during LA-ICP-MS data reduction. Indeed, the inclusions in olivine from garnet metaperidotite and chlorite harzburgite display reaction haloes in the host made of magnesian silicates (olivine and/or serpentine) against the host (Fig. 3a), pointing to post-entrapment interaction between fluid and olivine host.

Chlorite harzburgite. Inclusions were investigated in carbonate-free (Mg304-92-1) and carbonate-bearing chlorite harzburgite (Mg304-92-2), where magnesite and dolomite are peak and retrograde rock-forming minerals, respectively. Inclusions in olivine of the carbonate-free sample contain Fe-oxide, Cl-bearing phase and Ni sulfide (Fig. 5). The opaque minerals differ from those of inclusions in garnet for lower Cr content of oxide and for presence of Ni as main sulfide component (Tab. R3). Same as the garnet-hosed inclusions, the above opaque phases are associated with chlorite and serpentine. The latter locally appears to overgrow former olivine, showing a different electronic image but whose analysis was hampered by the small olivine size (Fig. 3b).

In the carbonate-bearing sample MG304-92-2 magnesite occurs as rock-forming mineral coexisting with high-pressure olivine, orthopyroxene and chlorite (Scambelluri et al., 2014, their Fig. 3a). It is overgrown by rims of retrograde dolomite. In this sample, magnesite also occurs as inclusion-forming mineral together with serpentine, chlorite, magnetite. Magnesite precipitation in inclusions indicates the presence of carbon species in the dehydration fluid within this sample. Interestingly, the inclusion magnesite also shows partial replacement by dolomite. This finding, together with evidence of inclusion-olivine replacement by serpentine, suggests precipitation of high-pressure phases within fluid-inclusions, followed by their replacement during back reaction with the inclusion fluid during retrograde metamorphism and exhumation.

6. Trace element compositions of inclusions

LA-ICP-MS analyses of inclusions in garnet metaperidotite and chlorite harzburgite are reported in Tables 1 and R4. The time-resolved analyses (Fig. 6) of inclusions hosted by garnet (Fig. 6a) and olivine (Figs. 6b; c; d) reveal detectable peaks in fluid-mobile elements and LILE. The inclusion compositions are portrayed in Figure 7 as spidergrams normalized to Primitive Mantle (PM, McDonough and Sun, 1995).

In garnet metaperidotite, the olivine-hosted inclusions display strongly elevated concentrations of Cs, Rb, Ba, Pb, As, Sb, Sr and Cl (up to 1000 PM) and moderate enrichments of B, U and partly Li (up to 10 PM; Fig. 7a). Because only a few of all trace elements returned significant concentrations for the host olivine (due to the smaller beam size employed for inclusion analysis and to the fact that detection limits negatively correlate with beam size), measured element distribution coefficients obtained from these analyses are limited. $KD_{(fluid/olivine)}$ for inclusion-host olivine pairs range considerably; hence, only orders of magnitude can be estimated (Si, Mg, Fe $\sim 10^1$, As $\sim 10^2$; Na, Sr, Pb $\sim 10^3$); however, Ti = 0.5 and Li = 4 are well constrained. An alternative approach is to estimate $KD_{(fluid/olivine)}$ values by combining the fluid data with large-beam (and thus low LOD) analyses of olivine from the same rock sample (published in Scambelluri et al., 2014). This approach returns $KD_{(fluid/olivine)}$ = 4 for Li (identical to that above), for B = 3 (consistent with Scambelluri et al., 2004a; Tenthorey and Hermann, 2004), for As = 350, for Sr = 33000, and for Sb = 1230. Even with large beam sizes, olivine analyses did not return significant concentrations for several elements. In such cases, miminum $KD_{(fluid/olivine)}$ values can be estimated based on the element-specific lower LOD values obtained (plotted in Fig. 8a with a vertical arrow pointing downwards). This way we obtain for Rb = 3500, for Cs = 10000, for Ba = 25000, for Y = 80, for La = 830, for Ce = 650, for Nd = 40, for Dy = 20, for Pb = 8300 and for U = 90. This strongly

325   suggests extreme LREE enrichments in fluids coexisting with olivine, very similar to fluid

326   patterns observed in the water-basalt system at 4-6 GPa (Kessel et al., 2005b).

327   The garnet-hosted inclusions of this sample are different (Fig. 7b). The LILE and fluid-

328   mobile element enrichments are less pronounced than for the olivine-hosted inclusions.

329   Cesium, Rb, B, As, Sb and Li show PM-normalized values above 1 while most other elements

330   are below 1. Significant measurements for elements in garnet were only obtained for MREE to

331   HREE, Li, and Nb. The few, directly determined element distribution coefficients show

332    $KD_{(fluid/garnet)}$ values between ca. 0.2 and 0.05 for the REE (decreasing with increasing

333   atomic number), and in the order of 10 for Li. $KD_{(fluid/garnet)}$ values for Sr and Nb are around

334   4 and 1.7, respectively. For the other elements, it is not useful to report minimum

335    $KD_{(fluid/garnet)}$ values, because the respective detection limits for these elements are at the

336   lower end of the ranges covered by the fluid element concentrations (compare with Tab. R4).

337   The olivine-hosted inclusions in chlorite harzburgite (MG204-92-2) are different from

338   the olivine-hosted inclusions in MG160-C1 and resemble those hosted by garnet in this

339   sample (Fig. 7c; Tab. 1). Concentrations relative to PM are again most enriched for As and Sb,

340   followed by Cs and B. Lead shows PM concentrations, and the other elements are variably

341   below PM values. As for garnet in MG160-C1, only a few of the host olivine element

342   concentrations are significant; most elements were below the respective LOD's. Estimated

343    $KD_{(fluid/olivine)}$ for As is about 100, while for B, Nb, Ta, Zr it is around 1 and for Li it is ~0.2.

344   Alltogether, prominent enrichments in As and Sb and variably enriched large ion

345   lithophile elements plus positive PM-normalized anomalies for B and partly Pb characterize

346   all inclusion compositions, while Sr is only enriched in the olivine-hosted inclusions of sample

347   MG160-C1. These olivine-hosted inclusions contain a prominent halogenide component

348   (~1.5wt% Cl) that is absent from inclusions hosted by garnet or in olivine from the chlorite

349   harzburgite (Tab. 1), thus demonstrating that two different fluid inclusion generations are

14

350 present in these samples. The least prominent relative LILE enrichment is revealed by olivine-

351 hosted inclusions of chlorite harzburgite MG304-92-2, consistent with the corresponding low

352 bulk rock values (Scambelluri et al., 2014) of 0.014µg/g Cs, 0.052µg/g Rb, 0.83µg/g Ba and

353 the depleted LREE concentrations (e.g., 0.085µg/g La) indicative of prominent melt depletion

354 prior to hydration.

355

356 **7. Discussion**

357 The garnet metaperidotite and chlorite harzburgite from Cima di Gagnone are the high-

358 pressure breakdown products of mantle rocks affected by multiple serpentinization stages,

359 oceanic and subduction-related (Evans and Trommsdorff, 1978; Scambelluri et al., 2014).

360 Positive anomalies in As, Sb, Be, elevated contents in radiogenic Sr, Pb and low $\delta^{11}B$

361 characterizing bulk rocks and high-pressure minerals point to exchange between the

362 serpentinzed peridotite precursors and the enclosing paragneiss during subduction burial

363 (Scambelluri et al., 2014; Cannaò et al., 2013). This geochemical record candidates Gagnone as

364 prime example of metaperidotitic slab lenses in subduction mélanges, or of slices of hydrated

365 supra-subduction zone mantle entrained into the subduction plate interface. In Gagnone, the

366 prograde dehydration evolution presented in the pressure-temperature diagrams of Figure 1

367 is indicated by relict (metastable) serpentine and chlorite + amphibole inclusions in eclogite-

368 facies minerals of chlorite harzburgite and garnet metaperidotite, respectively. This indicates

369 that chlorite harzburgite and garnet peridotite underwent antigorite breakdown that, in

370 garnet peridotite, was followed by chlorite dehydration (Fig. 1a, b).

371

372 *7.1. Inclusion textures and post-entrapment modifications*

373 The garnet- and olivine-hosted polyphase inclusions presented here further constrain

374 the dehydration process that affected the metaperidotite protoliths. In terms of texture, the

polyphase inclusions are comparable with primary and pseudosecondary fluid inclusions, i.e., randomly dispersed in the core of high-pressure minerals or as inclusion trails that do not intersect grain boundaries (Fig. 2e). Despite deriving from devolatilization reactions releasing water-rich fluids, the Gagnone inclusions do not correspond to liquid-rich aqueous fluids, but are filled with minerals. This indicates post-entrapment modifications that need to be addressed first.

Post-entrapment modifications can be isochemical and non-isochemical, and the latter need to be recognized in order to understand the significance of data. Post-entrapment crystallization in response to H or water loss does not pose analytical problems as long as the entire inclusion content is analyzed, as for example via drilling out complete inclusions from host minerals by LA-ICP-MS. Laboratory re-homogenization of inclusion contents (via reheating) is not viable because of H or water loss. Strictly, solvent loss qualifies the process of post-entrapment crystallization of eclogite-facies fluid inclusions as non-isochemical; however, the total dissolved solids load may remain unchanged. Non-isochemical post-entrapment modifications include diffusive equilibration with the host mineral or possibly with the surrounding rock materials and are indicated by magnetite crystallization in the inclusions. The model reaction fayalite (in olivine)+$H_2O \rightarrow SiO_{2(aq)}$ + magnetite + H^+, followed by H-loss, documents gain of Fe and increased f_{O2} in the fluid inclusion upon crystallization.

Evidence that mineral precipitation in inclusions began under elevated temperature (and high-pressure) conditions is provided by crystallization of olivine onto the inclusion walls, by olivine micro-crystals in inclusions (Fig. 3a,b), and by presence of magnesite in inclusions from magnesite-bearing chlorite harzburgite. The inclusion magnesite likely has lower Mg and higher Fe than the rock forming magnesite, though the small size of carbonate inside inclusions prevented satisfactory analytical work. Amphibole + spinel reaction rims associated with Cu-bearing sulfide occur in garnet-hosted inclusions, while the olivine-hosted

400   inclusions of the same sample and of MG304-92-2 contain Mg-silicates and Fe-Ni sulfides

401   without significant Cu (Figs. 4; 5). These Ni-bearing sulfides in the olivine-hosted inclusions

402   may be a reaction product with the olivine host. The differences in inclusion mineralogy may

403   therefore indicate post-entrapment interaction between inclusions and their host. These

404   interactions certainly affected major element fluid inclusion composition. However,

405   incompatible trace element patterns likely remain unaffected, in very much the same way as

406   for silicate melt inclusion (e.g., Danyushevsky et al., 2000; Pettke, 2006; Audetat and

407   Lowenstern, 2014) and as suggested by previous work on high-pressure polyphase inclusions

408   (e.g. Scambelluri et al., 2004a; Malaspina et al., 2006). Therefore, such high-pressure

409   polyphase inclusions can preserve important compositional information on the nature of

410   high-pressure fluids and document major fluid-processes during the subduction cycle.

411   The similarity to polyphase inclusions from the Almirez chlorite harzburgite is striking.

412   Both inclusion types contain chlorite, olivine (or serpentine), opaque minerals plus additional

413   minor phases (apatite in Almirez, chlorides in Gagnone; see Scambelluri et al., 2001).

414   Scambelluri et al. (2001; 2004a) estimate that the water-rich antigorite breakdown Almirez

415   fluid inclusions (with salinity between 0.4 and 2wt% NaCl) were desiccated by precipitation

416   of hydrous silicates and H$^+$ loss during during post-entrapment fluid inclusion modification.

417

418   *7.2 Fluid inclusion compositions*

419   Concerning fluid components, the elemental maps of Figures 4 and 5 and sulfide

420   analysis (Fig. 8) complement the inclusion compositional data and help identifying the

421   elements transported by the fluid. Elemental mapping sometimes revealed the presence of Cl,

422   often along with K and Fe. Chlorine anomalies only pertain to polyphase inclusions and are

423   absent in other rock domains. For this reason we propose that Cl was a high-pressure fluid

424   component, as pointed out by the significant Cl concentrations measured in olivine-hosted

17

425   inclusions from garnet peridotite MG160-C1 (Tab. 1). Serpentinite dehydration is known to

426   release chlorine-bearing fluids, especially during antigorite + brucite → olivine + H_2O reaction

427   (Scambelluri et al., 1997; 2004; Kodolanyi and Pettke, 2011). Scambelluri et al. (2004)

428   estimated a bulk loss of 2wt% H2O during this reaction. Chlorine concentrations in antigorite

429   dehydration fluids are lower (0.4-2wt% NaCl in fluid; Scambelluri et al., 2004a) because the

430   larger amount of water produced by the antigorite breakdown reaction (5 to 10wt% H_2O)

431   strongly dilutes the fluid. Presence of chlorine in the Gagnone polyphase inclusions therefore

432   confirms that dehydration of serpentinized ultramafic rocks releases Cl to fluids. The analysis

433   of sulfide at different textural sites of garnet peridotite and chlorite harzburgite points to a

434   change in sulfide composition during rock evolution, probably depending on fluid

435   composition. Figure 8 shows variation in sulfide composition from higher S and Fe

436   concentrations measured in rock-forming grains (mineral inclusions and interstitial

437   minerals), to lower Fe and S and higher Ni and/or Cu in sulfide crystals inside inclusions. In

438   the Gagnone metaperidotites, formation of sulfide phases that are not stable in pristine

439   mantle rocks and in altered seafloor mantle indicates sulfur mobility during subduction

440   metamorphism and suggests presence of reduced sulfur in the high-pressure fluids.

441   The presence of magnesite in inclusions from chlorite harzburgite provides compelling

442   evidence that, besides water, carbon is also a key component of the metaperidotite

443   dehydration fluid. Either decarbonation or magnesite dissolution was responsible for carbon

444   release into the aqueous deserpentization fluid. The available data do not constrain the C:O:H

445   abundance ratios of the fluid at entrapment conditions, however.

446

447   *7.2.1. Trace element inclusion compositions*

448   The trace element patterns of the fluid inclusion presented here suggest the presence of two

449   types of fluids in these rocks, one trapped in olivine of garnet peridotite MG160-C1 and one

450 trapped in garnet of this sample and in olivine of chlorite harzburgite MG304-92-2 (Fig. 7).

451 Olivine-hosted inclusions in MG160-C1 (type A; Fig. 7a) are quite enriched in fluid-mobile

452 elements (Cl, Pb, As, Sb, Tl, Cs, Rb, Ba; to a lesser extent B, Li and U) relative to primitive

453 mantle and to the type B fluid trapped in coarse garnet from the same sample (MG160-C1; Fig.

454 7b) and in olivine from chlorite harzburgite MG304-92-2 (Figure 7c; Tab. 1). However, the

455 PM-normalized patterns for the two fluid types are very similar (Fig. 9a) and show As, Sb,

456 ±Pb, ±Cs, ±Li above 1, but the latter fluid type appears much less enriched in fluid-mobile

457 elements. Type A fluid has up to 10^3 PM for Cl, Cs, Pb, As, Sb and $\sim 10^2$ PM for Tl, while Rb, Ba,

458 B, Sr are $\sim 10^1$ PM, and Na, K are ~ 2 PM. The combined enrichment of LILE and chalcophile

459 elements coincides with what is expected to be characteristic for a sediment-equilibrated

460 fluid. Type A fluid thus records a much more prominent sediment signal than does type B

461 fluid, a difference that can be related to multiple dehydration stages of rocks recording

462 different extents of pre-eclogitic interaction with sediment-derived fluids. In garnet

463 peridotite, fluid A and B in olivine- and in garnet-hosted inclusions, respectively, can be

464 related to different fluid-forming dehydration reactions and stages. Since the poikiloblastic

465 (rock-forming) and the vein-type garnet (Fig. 2a, b) crystallized late in these rocks, the garnet-

466 hosted inclusions can trap the fluid evolved during chlorite breakdown to garnet. Differently,

467 the olivine-hosted inclusions in the garnet metaperidotite may derive from earlier-stage,

468 antigorite dehydration (Fig. 1). In this perspective all olivine-hosted inclusions in garnet

469 metaperidotite (Fig. 9a) and in chlorite harzburgite (Fig. 9c) can derive from antigorite

470 breakdown: the different fluid-mobile elements concentrations of such inclusions (Figs. 7; 9)

471 can be related to variable intensities of precursor rock interaction with sediment-derived

472 fluids prior to eclogitic peak.

473   In summary, our analytical survey indicates that the chlorite harzburgite and the garnet

474 peridotite lenses from Gagnone trap fluids related to multiple dehydration stages recorded by

475   rocks affected by different degrees of interaction with sediment-derived fluid prior to

476   eclogitization.

477

478   *7.4. Relevance for trace element cycling in the subduction interface*

479   Presence of the same set of elements in the fluid-related inclusions and in high-

480   pressure minerals grown during metaperidotite dehydration implies a recycling process and

481   candidates the Gagnone metaperidotites as useful materials (i) for tracing fluid-mediated

482   trace element crust-mantle exchange, and (ii) for understanding the composition of

483   subduction fluids released by such a metasomatized mantle reservoir. The P-T conditions

484   metaperidotite recrystallization (800-850 °C; 3 GPa) fit recent modelling of top slab

485   temperatures in sub-arc subduction domains (Syracuse et al., 2010). The Gagnone fluid-

486   related inclusions are compared in Figure 10b with primary inclusions in chlorite harzburgite

487   from Cerro del Almirez (Scambelluri et al., 2004b). At both localities the inclusions display

488   comparable PM-normalized trace element patterns, showing positive spikes in fluid-mobile

489   Cs, Rb, Ba, B, Pb, Li (Fig. 9b; As and Sb data are not available for Almirez). From this

490   comparison it emerges that the de-serpentinization fluids in the two localities display

491   common features, represented by Cs, B, Pb and Li concentrations exceeding those of primitive

492   mantle. The PM-normalized pattern of the Gagnone fluid inclusions also compares well with

493   compositions of an antigorite breakdown fluid trapped in fluid inclusion during experimental

494   dehydration of natural serpentinite from Almirez (Fig. 9c) by Spandler et al. (2013). We thus

495   interpret these fluid data to represent a common serpentinite subduction fluid signature,

496   while prominent positive anomalies of As, Sb, Tl, Rb, Cs and Ba to this elemental budget

497   indicate input of a crustal (sedimentary) component to the de-serpentinization fluid.

498   Figure 7 shows that inclusions and host high-pressure minerals can have quite

499   different absolute trace element concentrations and patterns. This is the case for Cs, Rb, Ba, U

and Pb in olivine-hosted inclusions, showing high concentrations in such elements (up to

hundreds times the PM in olivine-hosted inclusions from garnet metaperidotite) that are

virtually absent in the mineral host. In such inclusions As, Sb and Tl are quite abundant. The

same reasoning can be applied to Cs, B, As and Li in garnet-hosted inclusions. This different

behaviour encourages the use of mineral/fluid partition coefficients (Fig. 9d), calculated for

several elements using the average compositions of polyphase inclusions (Table 1) and of

mineral hosts (see section 6). As expected, garnet has affinity for Zr, Y, HREE whereas olivine

can retain significant Li and B, as shown by $KD_{(fluid/olivine)}$ close to 3 and 4, as also documented

in previous studies (Tenthorey and Hermann, 2004; Scambelluri et al., 2004a). This fact was

already underlined for the Almirez chlorite harzburgite, hosting unexpectedly high amounts

of fluid-mobile elements, even noble gases, expected to preferentially leave the solid phases

during dehydration processes (Scambelluri et al., 2001, 2004a: John et al., 2011; Kendrick et

al., 2011). Therefore, the dehydrated, high-pressure metaperidotite residues can introduce

fluid-mobile element anomalies in the convecting mantle.

Arsenic, Sb, Be and part of the whole-rock Pb, B, Sr of the Gagnone metaperidotite were

acquired via exchange with metasedimentary country rocks during subduction burial

(Scambelluri et al., 2014; Cannaò et al., 2013). The capacity of serpentinized mantle to

incorporate fluid-mobile elements was emphasized by Hattori and Guillot (2003) and by

Deschamps et al. (2011), showing that As, Sb, B lost from dehydrating slabs at relatively low-

temperature are transferred to altered ultramafic (mantle) lithologies. The high

concentrations of such fluid-mobile elements measured in the Gagnone bulk rocks, fluid-

related inclusions and high-pressure minerals fits the above interpretation, and points out

that As, Sb, Cs, Rb, Tl (together with radiogenic Pb and Sr; Cannaò et al., 2013) were *fluid-*

transported' from the country paraschist into the mélanged ultramafic bodies. The

compositions of the hydrated Gagnone metaperidotite protoliths are reconstructed in Figure

9e using the mineral/fluid partition coefficients of Figure 9d, together with the modal amounts of rock-forming olivine and garnet in garnet metaperidotite (amphibole, ortho and clinopyroxene have been omitted from this estimate due to a lack of coupled fluid inclusion and host measurements). Figure 9e shows that the trace element patterns of abyssal, mantle wedge and subduction-zone serpentinites (Deschamps et al., 2013) and of the Gagnone garnet metaperidotite protoliths are comparable, the main difference being much higher absolute concentrations of Cs, Rb, Ba, La, CePb, As, Sb, Sr, Nd of the Gagnone rocks prior to dehydration. Because of the magnitude of these differences, the Cima di Gagnone garnet metaperidotite pattern emphasizes the crustal (sedimentary) input recorded by these rocks. Therefore, they may represent an ultramafic end-member for uptake of crust-derived elements.

The local-scale trace element transfer documented here for Gagnone may have larger-scale implications when considering slab to supra-subduction zone mantle transfer of fluids and elements. A possible interpretation arising from Figure 9b is that Almirez, like Gagnone, underwent fluid-mediated element exchange with associated crustal rocks prior to antigorite breakdown. Crustal gneisses crop out quite close to the Almirez ultramafic body: input from external (sedimentary) reservoirs into serpentinites has been recently advocated by Marchesi et al. (2013) and Harvey et al. (2014) based on trace element and Sr isotopic studies. This may better explain the enrichment in crust-derived elements unusual in serpentinites formed by single-stage ocean floor hydration, and increasingly found in ultramafic rocks evolved through subduction zone processes. If one extrapolates from the context of top-slab mélange environment, and considers the pre-dehydration Gagnone compositions (Fig. 9e) as representative of altered supra-subduction mantle wedge, the potential of ultramafic rock systems in storing and transporting slab-derived elements from shallow (forearc) to deep subduction settings becomes compellingly apparent. As stated previously (Hyndman and Peacock, 2003; Savov et al., 2005; Hattori and Guillot, 2003; Scambelluri and Tonarini, 2012)

550 the shallow-level water transfer from slab to overlying mantle coincides with fluid-mobile

551 element transport. Cannaò et al. (2013) show that this transfer also regards radiogenic Sr and

552 Pb isotopes. Gagnone may therefore represent a highly enriched end-member of this process.

553

554 **8. Conclusions**

555 The Gagnone metaperidotite suite presented here derives from precursor mantle rocks

556 recording: (i) early element uptake during oceanic hydration followed by exchange with

557 sediment-derived fluids during subduction burial; (ii) eclogite-facies dehydration

558 (Scambelluri et al., 2014). The investigated chlorite harzburgite essentially records high-

559 pressure breakdown of serpentine, whereas the associated garnet metaperidotite records a

560 first event of de-serpentinzation followed by chlorite breakdown to garnet.

561   The eclogite-facies olivine and garnet trap primary to pseudosecondary inclusions

562 representing the fluid evolved during breakdown of antigorite (fluid A) and chlorite (fluid B).

563 The inclusions contain fluid-mobile elements (high Cl, S; variable Cs, Rb, Ba, B, Pb, As, Sb).

564 Presence of magnesite in inclusions from metaperidotite samples showing rock-forming

565 eclogitic magnesite indicates carbon release to the aqueous fluid via decarbonation and/or

566 dissolution.

567   The olivine-hosted inclusions in the garnet metaperidotite (fluid A) have the highest fluid-

568 mobile element content and LREE, reflecting a sedimentary signal and the recycling

569 sedimentary components into the de-serpentinization fluid. Lower degrees of enrichments of

570 these elements in olivine-hosted inclusions from chlorite harzburgite point to variable

571 degrees of pre-eclogitic alteration of the Gagnone rocks.

572   The inclusions trapped in garnet (fluid B, deriving from chlorite dehydration) display

573 relatively low fluid-mobile elements, suggesting squeezing of a rock that already delivered

574 such components during serpentine breakdown.

575   Our observations indicate that altered supra-subduction mantle sequesters water, carbon

576   and fluid-mobile elements sourced by slabs, and that dehydration of such a metasomatized

577   mantle provides fluid-mobile element-enriched fluids (like the Gagnone inclusions) to arcs.

578   We confirm the tendency of serpentinized mantle to capture fluid-mobile elements and

579   propose that through fluid-mediated transfer from sediments combined with subduction-

580   zone processing, serpentinzed mantle acts as carrier of specific elements to arcs.

581   The shallow element release from slabs to mantle, its downward flow and its subsequent

582   (subarc) dehydration tranfers the goods to subarc mantle (Hyndman and Peacock, 2003;

583   Ruepke et al., 2004; Savov et al., 2004; Scambelluri and Tonarini, 2012) without need of

584   concomitant subarc dehydration/melting of metasedimentary slab components. Therefore,

585   we conclude that the Gagnone inclusions can represent what is sourced by slab-contaminated

586   mantle peridotite in deep subduction settings.

587

591

References

Alt J.C, Schwarzenbach E.M., Früh-Green G.L., Shanks W.C.III, Bernasconi S.M., Garrido C.J., Crispini L., Gaggero L., Padrón-Navarta J.A., Marchesi C. (2013) The role of serpentinites in cycling of carbon and sulfur: Seafloor serpentinization and subduction metamorphism. Lithos 178, 40-54a

Angiboust S., Pettke T., De Hoog C.J.M., Caron B., Onken O. (2014) Channelized fluid flow and eclogite-facies metasomatism along the subduction shear zone. Journal of Petrology 55, 883-916.

Audetat, A, Lowenstern, J. B. (2014) Melt inclusions. Treatise on Geochemistry, Second Edition, (2014), vol. 13, pp. 143-173.

Bebout, G.E. (2007). Metamorphic chemical geodynamics of subduction zones. *Earth and Planetary Science Letters* **260**, 373–393

Blanco-Quintero, I.F., García-Casco, A., Gerya T.V. (2011) Tectonic blocks in serpentinite mélange (eastern Cuba) reveal large-scale convective flow of the subduction channel. *Geology* 39, 79-82doi:10.1130/G31494.

Boschi C., Bonatti E., Ligi M., Brunelli D., Cipriani A., Dallai L., D'Orazio M., Früh-Green G.L., Tonarini S., Barnes J.D., Bedini R.M. (2013) Serpentinization of mantle peridotites along an uplifted lithospheric section, Mid Atlantic Ridge at 11° N. Lithos 178, 3-23.

Bostock, M.G., Hyndman, R.D., Rondenay, S. & Peacock, S.M. (2002). An inverted continental Moho and serpentinization of the forearc mantle. *Nature* **417**, 536-538.

Cannaò, E., Scambelluri, M., Agostini, S., Tonarini, S. (2014) The geochemical fingerprint of

619   serpentinite- and crust-dominated plate-interface settings: some tectonic implications. Geophysical

620   Research Abstracts Vol. 16, EGU2014- EGU General Assembly 2014

621

622   Cannat, M., Mével, C., Maia, M., Deplus, C., Durand, C., Gente, P., Agrinier, P., Belarouchi, A., Dubuisson,

623   G., Humler, E. & Reynolds, J. (1995). Thin crust, ultramafic exposures, and rugged faulting patterns at

624   the Mid-Atlantic Ridge (22°–24°N). *Geology* **23**, 49–52.

625

626   Danyushevsky, L.V., Della-Pasqua, F.N. & Sokolov, S. (2000): Re-equilibration of melt inclusions

627   trapped by magnesian olivine phenocrysts from subduction-related magmas: petrological

628   implications. Contrib. Min. Petrol. 138(1), 68–83.

629

630   De Hoog J.C.M., Hattori K., Jung H. (2014) Titanium- and water-rich metamorphic olivine in high-

631   pressure serpentinites from the Voltri Massif (Ligurian Alps, Italy): evidence for deep subduction of

632   high-field strength and fluid-mobile elements. Contributions to Mineralogy and Petrology 167, 990.

633

634   Deschamps, F., Guillot, S., Godard, M., Chauvel, C., Andreani, M. & Hattori, K.H. (2010). In situ

635   characterization of serpentinites from forearc mantle wedges: timing of serpentinization and behavior

636   of fluid-mobile elements in subduction zones. *Chemical Geology* **269**, 262–277.

637

638   Deschamps, F., Guillot, S., Godard, M., Andreani, M. & Hattori, K.H. (2011). Serpentinites act as sponges

639   for fluid-mobile elements in abyssal and subduction zone environments. *Terra Nova* **23**, 171–178.

640

641   Deschamps, F., Godard, M., Guillot, S., Hattori, K. (2013) Geochemistry of subduction zone

642   serpentinites: A review. Lithos 178, 96–127.

643

644   Dvir, O., Pettke, T., Fumagalli, P., and Kessel, R., 2011. Fluids in the peridotite-water system up to 6 GPa

645   and 800 degrees C: new experimental constrains on dehydration reactions. Contributions to

646   Mineralogy and Petrology 161, 829-844.

647

648   Eggins, S. M. and Shelley, J. M. G., 2002. Compositional heterogeneity in NIST SRM 610-617 glasses.

649   Geostandards Newsletter-the Journal of Geostandards and Geoanalysis 26, 269-286.

650

651   Engi, M., Berger, A. & Roselle, G.T. (2001). Role of the tectonic accretion channel in collisional orogeny.

652   *Geology* **29**, 1143–1146.

653

654   Evans, B.W. & Trommsdorff, V. (1978). Petrogenesis of garnet lherzolite, Cima di Gagnone, Lepontine

655   Alps. *Earth and Planetary Science Letters* **40**, 333-348

656

657   Evans, B.W. & Trommsdorff, V. (1983). Fluorine hydroxyl titanian clinohumite in alpine recrystallized

658   garnet peridotite: compositional controls and petrologic significance. *American Journal of Science* **283-**

659   **A** 355-369.

660

661   Evans K.A., Tomlins A.G., Cliff J., Fiorentini M. (2014) Insights into subduction zone sulfur recycling

662   from isotopic analysis of eclogite-hosted sulfides. Chemical Geology 365, 1-19

663

664   Federico, L., Crispini, L., Scambelluri, M. & Capponi G. (2007). Ophiolite mélange zone records

665   exhumation in a fossil subduction channel. *Geology*, 35 499-502.

666   Früh-Green G.L., Connolly J.A.D, Kelley D.S., Plas A. and Grobéty B. (2004) Serpentinization of oceanic

667   peridotites: Implications for geochemical cycles and biological activity. *In: The Subseafloor Biosphere at*

668   *Mid-Ocean Ridges,* eds W.D. Wilcock, D.S.Kelley, E. DeLong, C. Cary, *AGU Geophysical Monograph*

669   144:119-136.

670   Fumagalli, P. & Poli, S. (2005). Experimentally determined phase relations in hydrous peridotites to

671   6.5 GPa and their consequences on the dynamics of subduction zones. *Journal of Petrology* **46**, 555-

672   578.

673

674   Fumasoli, M.W., 1974, Geologie des Gebietes no¨rdlich und sudlich der Jorio-Tonale-Linie im Westen

675   von Gravedona (Como, Italia). Dissertation thesis, Zurich, Universitat Zurich, 230 p.

676

677   Gerya, T.V., Stöckhert, B. & Perchuk, A.L. (2002). Exhumation of high-pressure metamorphic rocks in a

678   subduction channel: A numerical simulation. *Tectonics* **21**(6), 1056, doi: 1029/2002TC001406.

679

680   Harvey J., Garrido C.J., Savov I., Agostini S., Padrón-Navarta J.A., Marchesi C., Sánchez-Vizcaíno Sánchez-

681   Vizcaíno V., Gómez-Pugnaire M.T. (2014) 11B-rich fluids in subduction zones: The role of antigorite

682   dehydration in subducting slabs and boron isotope heterogeneity in the mantle. Chemical Geology 376,

683   20-30.

684

685   Hattori, K.H. & Guillot, S. (2003). Volcanic fronts form as a consequence of serpentinite dehydration in

686   the forearc mantle wedge. *Geology* **31**, 525-528.

687

688   Heinrich, C.A. (1982). Kyanite-eclogite to amphibolite facies evolution of hydrous mafic and pelitic

689   rocks, Adula nappe, Central Alps. *Contributions to Mineralogy and Petrology* **81**, 30–38.

690

691   Heinrich, C.A. (1986). Eclogite facies regional metamorphism of hydrous mafic rocks in the Central

692   Alpine Adula nappe. *Journal of Petrology* **27**, 123–154.

693

694   Hyndman, R.D. & Peacock, S.M. (2003). Serpentinization of the forearc mantle. *Earth and Planetary*

695   *Science Letters* **212**, 417–432,

696

697   Iwamori, H. (1998) Transportation of H_2O and melting in subduction zones. *Earth and Planetary*

698   *Science Letters* 160*,* 65–80

699   John, T., Scambelluri, M., Frische, M., Barnes, J. & Bach, W. (2011). Dehydration of subducting

700   serpentinite: Implications for halogen mobility in subduction zones and the deep halogen cycle: *Earth*

701   *Planetary Science Letters* **308**, 65-76.

702

703   Kendrick, M.A., Scambelluri, M., Honda, M. & Phillips, D. (2011). High abundance of noble gas and

704   chlorine delivered to the mantle by serpentinite subduction. *Nature Geoscience* **4**, 807-812.

705

706   Kessel, R., Schmidt, M. W., Ulmer, P. & Pettke, T. (2005a). Trace element signature of subduction-zone

707   fluids, melts and supercritical liquids at 120-180 km depth. *Nature* **437**, 724-727.

708   Kessel et al 2005 b

709

710   Kodolányi, J., Pettke, T., Spandler, C., Kamber, B.S. and Gméling, K. (2012) Geochemistry of ocean floor

711   and forearc serpentinites: Constraints on the ultramafic input to subduction zones. J. Petrol. 53, 235-

712   270.

713

714   Kodolanyi, J. and Pettke, T., 2011. Loss of trace elements from serpentinites during fluid-assisted

715   transformation of chrysotile to antigorite - An example from Guatemala. Chemical Geology 284, 351-

716   362.

717

718   Malaspina, N., Hermann, J., Scambelluri, M., Compagnoni, R. (2006) Polyphase inclusions in garnet-

719   orthopyroxenite (Dabie Shan, China) as monitors for metasomatism and fluid-related trace element

720   transfer in subduction zone peridotite. *Earth and Planetary Science Letters* 240, 668–680.

721

722   Marchesi C. Garrido C.J., Padrón-Navarta J.A., López Sánchez-Vizcaíno V, Gómez-Pugnaire M.T. (2013)

723   Element mobility from seafloor serpentinization to high-pressure dehydration of antigorite in

724   subducted serpentinite: Insights from the Cerro del Almirez ultramafic massif (southern Spain). Lithos

725   178, 128-142

726

727   McDonough, W.F. & Sun, S.-S., 1995. The composition of the Earth. *Chemical Geology* **120**, 223-253.

728

729   Möckel, J.R. (1969): Structural petrology of the garnet peridotite of Alpe Arami (Ticino, Switzerland).

730   *Leidse Geol. Meded.* **42**, 61–130.

731

732   Nimis, P. & Trommsdorff, V. (2001). Revised thermobarometry of Alpe Arami and other garnet

733   peridotites from the Central Alps. *Journal of Petrology* **42**, 103–115.

734

735   Pettke, T., Oberli, F., Audetat, A., Guillong, M., Simon, A. C., Hanley, J. J., and Klemm, L. M., 2012. Recent

736   developments in element concentration and isotope ratio analysis of individual fluid inclusions by

737   laser ablation single and multiple collector ICP-MS. *Ore Geology Reviews* **44**, 10-38.

738

739   Pfiffner, M. & Trommsdorff, V. (1998). The high-pressure ultramafic-mafic-carbonate suite of Cima

740   Lunga-Adula, Central Alps: excursions to Cima di Gagnone and Alpe Arami. *Schweizerische Mineral.*

741   *Petrogr. Mitt* **78**, 337-354.

742

743   Pluemper, O., John, T, Podldchikov, Y.Y. , Scambelluri, M. (2013) Self-organizing reactive porosity

744   waves allow large-scale fluid escape from subducting oceanic lithosphere. Goldschmidt2013

745   Conference Abstracts pg. 1973

746   Ruepke, L.H, Phipps Morgan, J., Hort, M., Connolly, J.A.D (2004). Serpentine and the subduction zone

747   water cycle. *Earth and Planetary Science Letters* 223, 17–34

748   Savov, I.P., Ryan, J.G., D'Antonio, M., Kelley, K. & Mattie, P. (2005). Geochemistry of serpentinized

749   peridotites from the Mariana Forearc Conical Seamount, ODP Leg 125: Implications

750   for elemental recycling at subduction zones: *Geochemistry, Geophysics, Geosystems* **6**, Q04J15,

751   doi:10.1029/2004GC000777.

752

753 Scambelluri, M., Piccardo, G.B., Philippot, P., Robbiano, A. & Negretti L. (1997). High salinity fluid

754 inclusions formed from recycled seawater in deeply subducted alpine serpentinite. *Earth and Planeary*

755 *Science Lett*ers **148**, 485-500.

756

757 Scambelluri M., Bottazzi P., Trommsdorff V., Vannucci R., Hermann J., Gòmez-Pugnaire M.T. & Lòpez-

758 Sànchez Vizcaino V. (2001). Incompatible element-rich fluids released by antigorite breakdown in

759 deeply subducted mantle. *Earth and Planeary Science Lett*ers **192**, 457-470.

760

761 Scambelluri M., Müntener O., Ottolini L., Pettke T. & Vannucci R. (2004a). The fate of B, Cl and Li in the

762 subducted oceanic mantle and in the antigorite-breakdown fluids*. Earth and Planetary Science Letters*

763 **222**, 217-234.

764

765 Scambelluri M., Fiebig J., Malaspina N., Müntener O. & Pettke T., (2004b). Serpentinite subduction:

766 Implications for fluid processes and trace-element recycling. *International Geology Reviews* **46**, 595-

767 613.

768

769 Scambelluri, M., Pettke, T., and van Roermund, H. L. M., 2008. Majoritic garnets monitor deep

770 subduction fluid flow and mantle dynamics. Geology 36, 59-62.

771

772 Scambelluri M. & Tonarini S. (2012). Boron isotope evidence for shallow fluid transfer

773 acrosssubduction zones by serpentinized mantle. *Geology* **40**, n. 10, 907-910.

774

775 Scambelluri M., Pettke T., Rampone E. Godard M, Reusser E. 2014. Petrology and trace element budgets

776 of high-pressure peridotites indicate subduction dehydration of serpentinized mantle (Cima di

777 Gagnone, Central Alps, Switzerland). Journal of Petrology 55, 459-498.

778

779   Schmid, S.M., Rück, P. & Schreurs, G. (1990): The significance of the Schams nappes for the

780   reconstruction of the palaeotectonic evolution of the Penninic zone along the NRP20-East traverse

781   (Grisons, Eastern Switzerland). *Mémoires Societè Géologique Fr*ance **156**:263–287.

782

783   Sharp, Z.D. & Barnes, J.D. (2004). Water-soluble chlorides in massive seafloor serpentinites: a source of

784   chloride in subduction zones. *Earth and Planetary Science Letters* **226**, 243–254.

785

786   Shimizu, N., Scambelluri, M., Santiago Ramos, D., Tonarini, S. (2013). Boron and sulfur isotopic

787   variations during subduction of hydrated lithosphere: The Erro Tobbio case. *Mineralogical Magazine*

788   **77** (5), 2201.

789

790   Spandler, C., Pettke, T., and Rubatto, D., 2011. Internal and External Fluid Sources for Eclogite-facies

791   Veins in the Monviso Meta-ophiolite, Western Alps: Implications for Fluid Flow in Subduction Zones.

792   *Journal of Petrology* **52**, 1207-1236.

793

794   Spandler C., Pettke T., Hermann J. (2014) Experimental study of trace element release during

795   ultrahigh-pressure serpentinite dehydration. Earth and Planetary Science Letters 391, 296-306

796

797   Syracuse, E.M., van Keken, P.E., Abers, G.A., 2010. The global range of subduction zone thermal models.

798   Phys. Earth Planet. Int. 183, 73-90.

799

800   Tenthorey, E. & Hermann, J. (2004). Composition of fluids during serpentinite breakdown in

801   subduction zones: evidence for limited boron mobility. *Geology* **32**, 865–86

802

803   Trommsdorff, V., 1990, Metamorphism and tectonics in the Central Alps: The Alpine lithospheric

804   mélange of Cima Lunga and Adula. *Società Geologica Italiana, Memorie*. **45**, 39–49.

805

806 Trommsdorff, V., López Sánchez-Vizcaíno, V., Gómez-Pugnaire, M.T., Müntener, O. (1998). High

807 pressure breakdown of antigorite to spinifex-textured olivine and orthopyroxene, SE Spain.

808 *Contributions to Mineralogy and Petrology* **132**, 139–148.

809

810 Ulmer, P., Trommsdorff, V., 1995. Serpentine stability to mantle depths and subduction related

811 magmatism. *Science* 268, 858–861.

812

813 Ulmer, P. & Trommsdorff, V. (1999). Phase relations of hydrous mantle subducting to 300 km. In: Fei Y,

814 Bertka CM, Mysen BO (eds) Mantle petrology: field observations and high pressure experimentation.

815 Special Publication No. 6. The Geochemical Society, Houston, pp 259–281

816

817 Wunder B. and Schreyer W. (1997) Antigorite: High-pressure stability in the system $MgO-SiO_2-H_2O$

818 (MSH). Lithos 41, 213-227.

819

820

821

822 **Figure Captions**

823

824 Figure 1. Pressure-Temperature pseudosections for the Gagnone garnet peridotite (A) and

825 chlorite harzburgite (B) (after Scambelluri et al., 2014). Arrows show possible prograde paths

826 joining early stage assemblages, defined by monophase inclusions in high-pressure minerals,

827 with the stability filed defined for peak eclogite-facies parageneses. Garnet peridotite in (A)

828 records antigorite and chlorite breakdown. C: As-Sb diagram showing the array of high-

829 pressure minerals and bulk rocks from Gagnone, comprised between Primary Mantle

830 reservoirs and pelagic clays (after Scambelluri et al., 2014).

831

832   Figure 2. Textures of garnet peridotite (A and B) and of polyphase inclusions in garnet (C to F)

833   (sample MG 160 C1). Rocks contain garnet megacrystals likely representing fluid pockets in

834   garnet peridotite. F: close up of polyphase inclusions in garnet.

835

836   Figure 3. (A) and (B): scanning electron microscope images of olivine-hosted inclusions from

837   garnet peridotite and chlorite harzburgite, respectively. (A) shows an olivine reaction halo

838   between the inclusion and the olivine host. (B) shows an olivine microcrystal inside the

839   inclusion being replaced by serpentine. (c) and (D) are Mg and Si elemental maps of an olivine

840   hosted inclusion showing a continuous reaction rim of a Mg-silicate phase between inclusion

841   and host mineral.

842

843   Figure 4. Rock textures: (A) illustrates chlorite harzburgite showing an olivine +

844   orthopyroxene + chlorite + magnesite paragenesis. B shows interstitial sulphide (lower left

845   side of the picture) in between high-pressure minerals and coarse sulphide inclusion in

846   chlorite harzburgite minerals. C: primary polyphase inclusions in high-pressure olivine from

847   chlorite harzburgite. D: close up of polyphase inclsuions in olivine.

848

849   Figure 5. Elemental maps, showing element distribution inside polyphase inclusions hosted in

850   garnet. Garnet peridotite sample MG 160C1.

851

852   Figure 6. Elemental maps, showing element distribution inside polyphase inclsuions hosted in

853   olivine. Garnet peridotite sample MG 160C1, and chlorite harzburgite sample MG304 92-2.

854

855   Figure 7. Time-resolved fluid inclusion analyses. (A) is hosted by garnet, sample MG160-C1,

856   (B) is hosted by olivine, sample MG304-92-2, and (C,D) shows the same inclusion hosted in

857   olivine, sample MG160-C1.

858

859

860   Figure 8. PM-normalized trace element compositions of polyphase inclusions and of their

861   hosts in olivine (A) and garnet (B) from garnet peridotite and in olivine (C) from chlorite

862   harzburgite samples. Downward pointing arrows in (A) identify the respective limits of

863   detections for host olivine analyses. See text for implications regarding the two fluid types (A

864   in olivine and B in garnet) from the garnet perditotite.

865

866   Figure 9. Plots of Ni+Cu and S vs. Ve of of rock- and of inclusion-forming sulfides.

867

868   Figure 10. A: composition of all analysed inclusions. B: trace element patterns of Gagnone and

869   Almirez inclusions. Only reported are the element common to the two sample sets. Almirez

870   inclusion data are from Scambelluri et al. (2004b). C: trace element patterns of Gagnone

871   inclusions and of the experimental antigorite-breakdown to fluid inclusions in the P-T range

872   of 3.5-4 GPa and 700-900 °C (Spandler et al., 2014).

873

874   Figure 11. A: Mineral/fluid trace element partition coefficients (measured for fluid - host

875   mineral pairs in black and minimum KD estimated from fluid inclusion data combined with

876   mineral analyses from the same rock in grey symbols) for garnet peridotite. B: estimated

877   composition of the Gagnone garnet peridotite prior to eclogite facies antigorite dehydration.

878   The reconstructed composition only accounts for garnet and olivine, being the only phases for

879   which fluid-mineral host partition coefficients are available.

The Gagnone metaperidotites record multistage subduction metasomatism and dehydration.

They trap inclusions of fluids evolved during breakdown of antigorite and of chlorite.

The trace element compositions of such fluids indicate recycling of sedimentary components

Altered subduction-zone mantle uptakes and delivers sediment-derived elements to fluids

This transfer process may not require concomitant subarc dehydration of slab metasediment
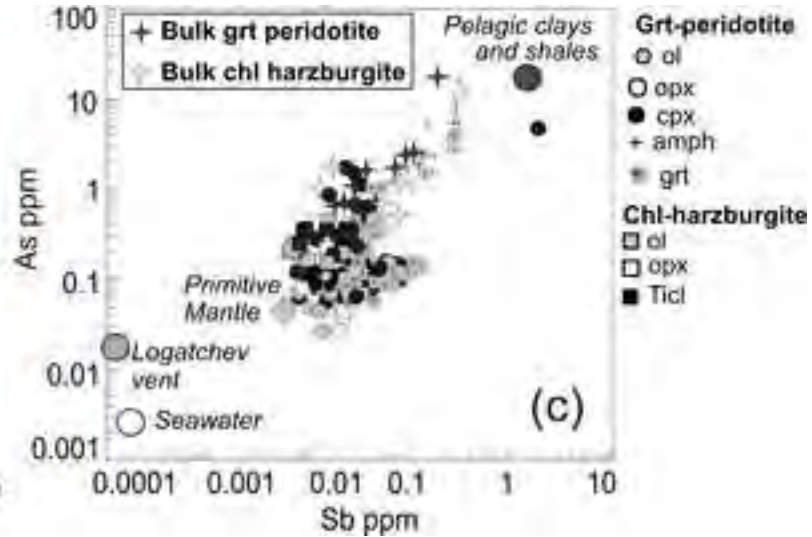
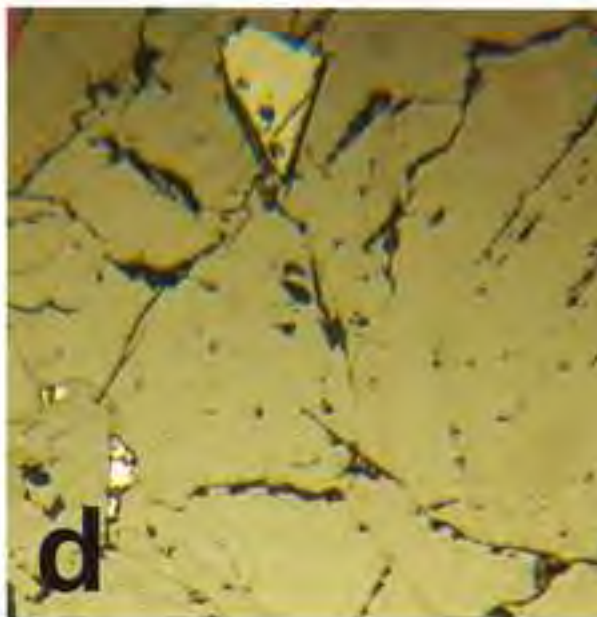**Figure 2**
Click here to download high resolution image
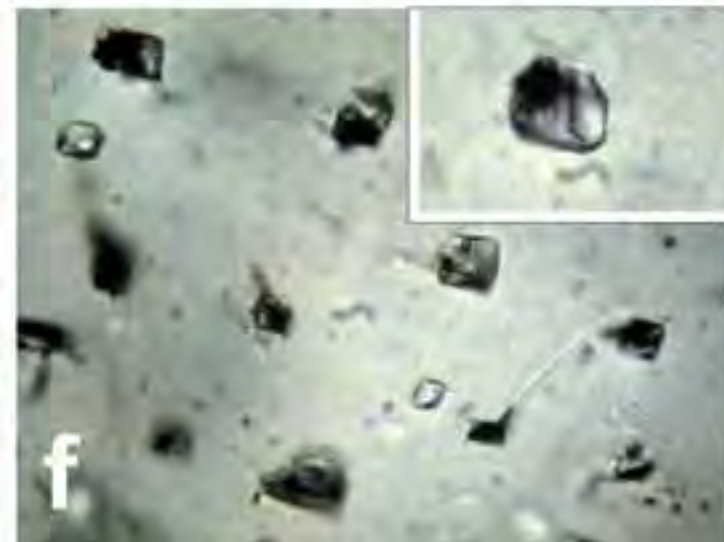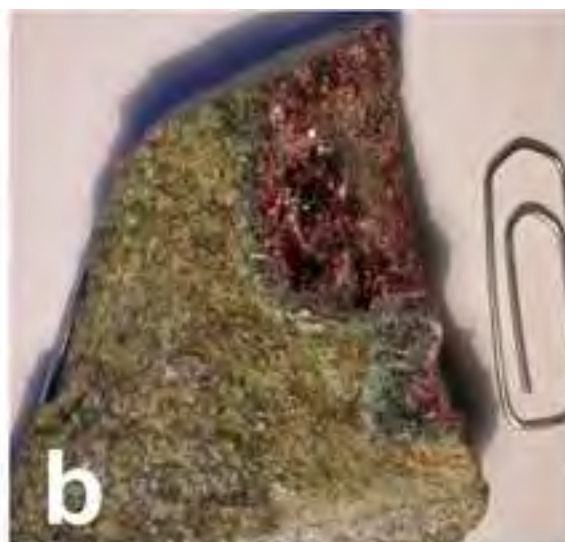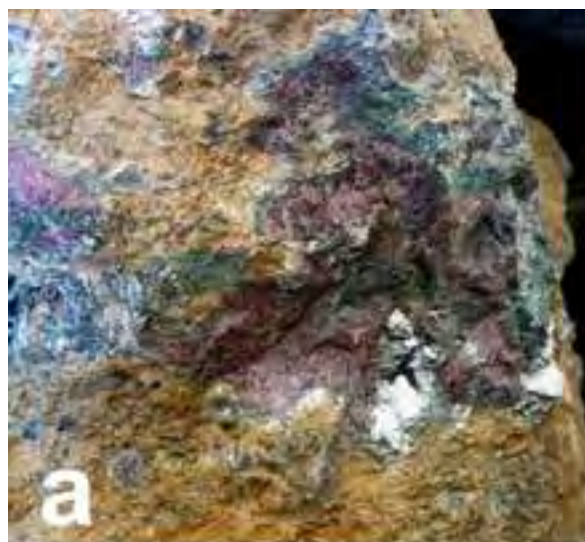
Figure 3
Click here to download high resolution image
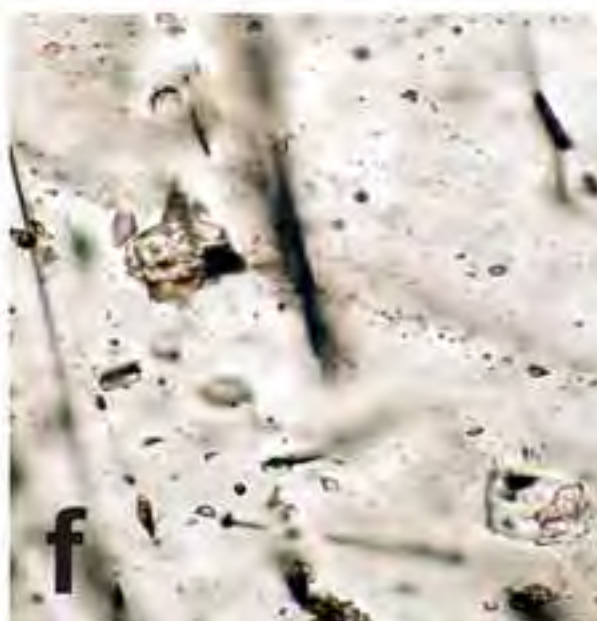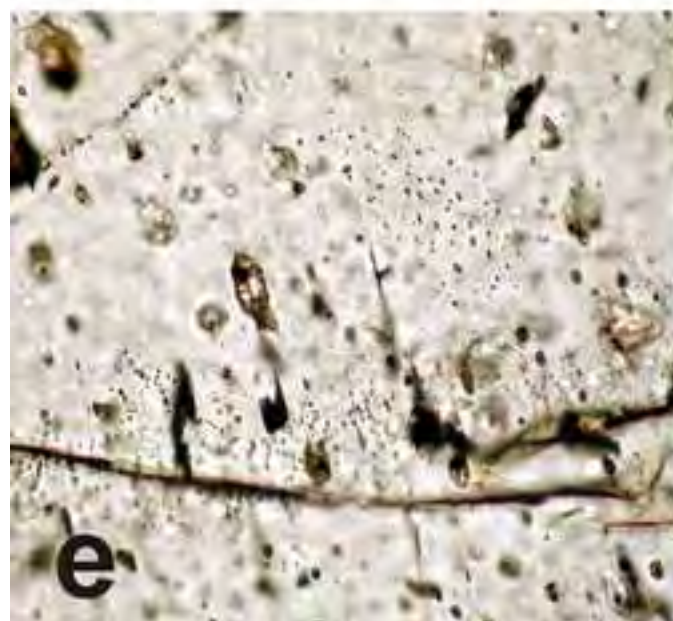
Garnet peridotite Mg160

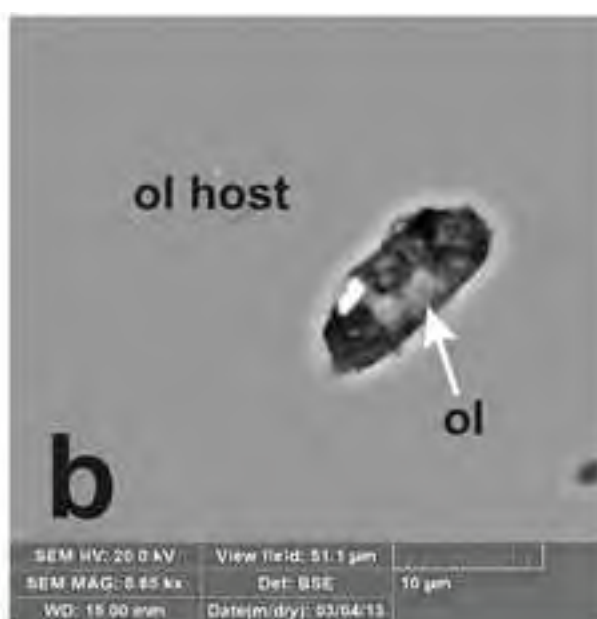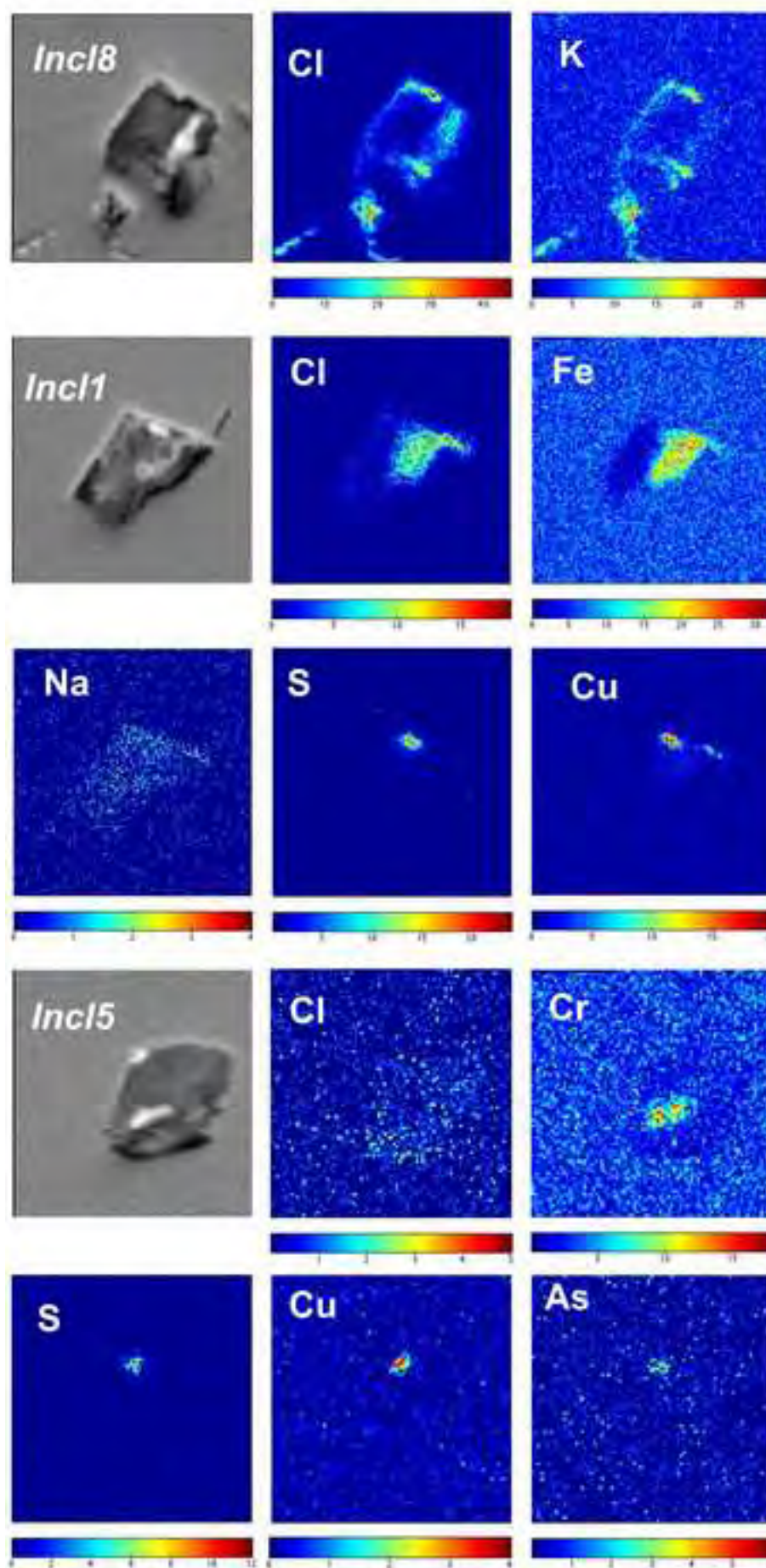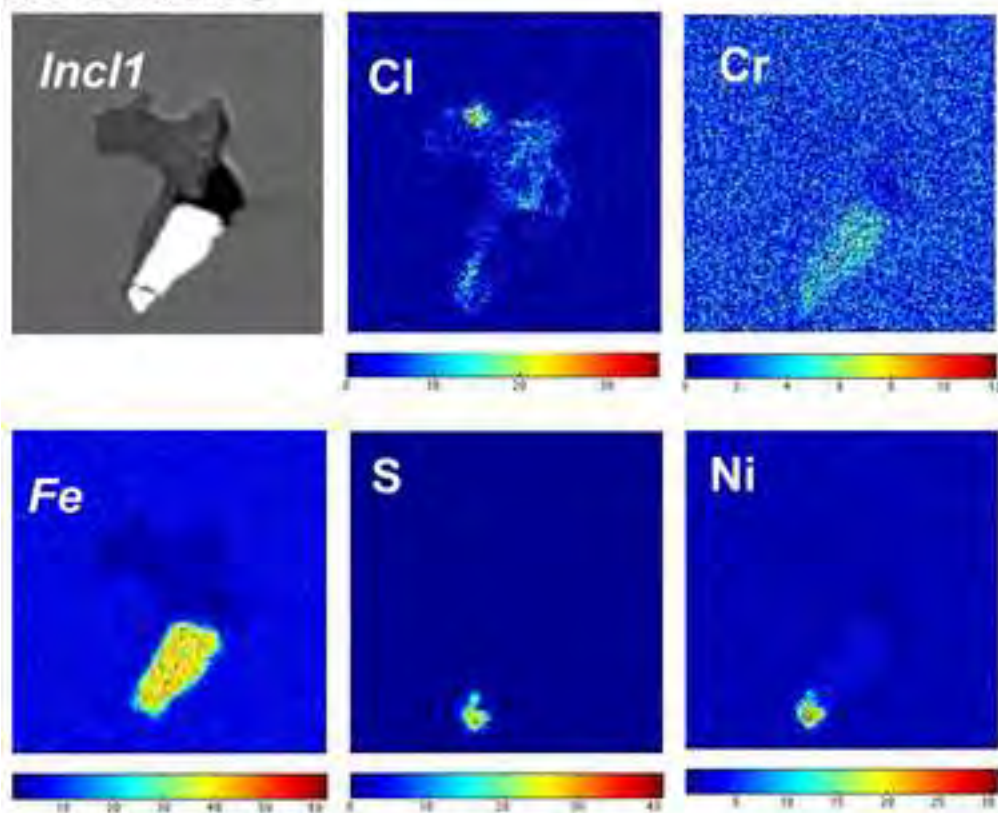Garnet peridotite Mg160 incs in olivine
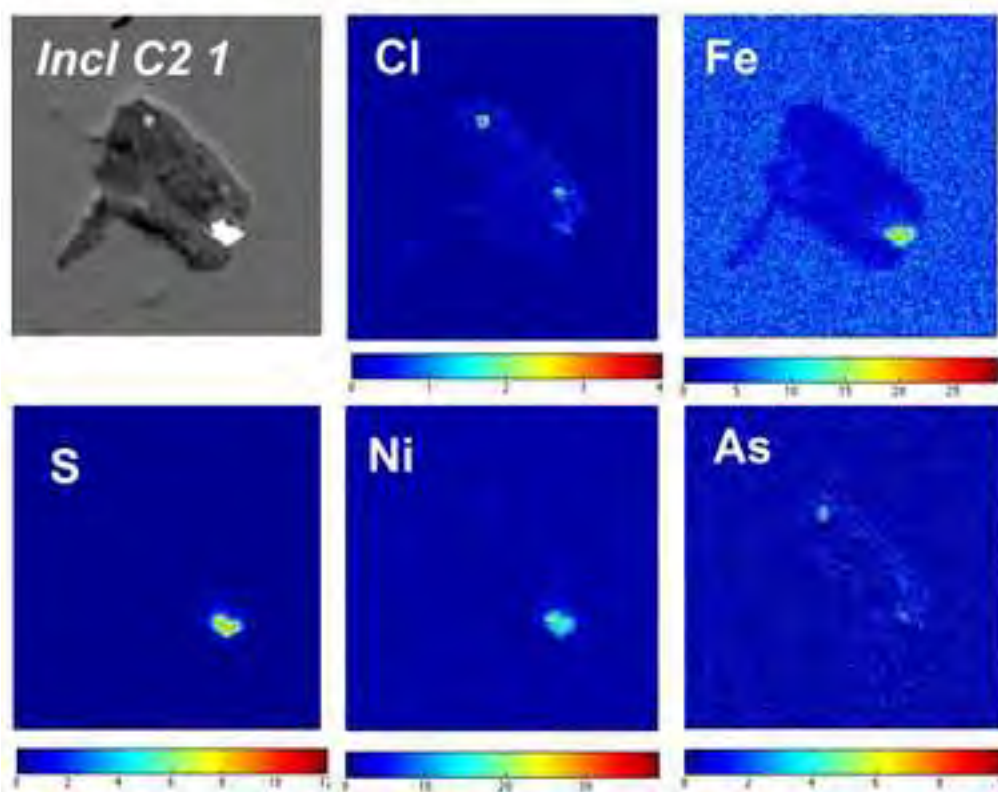
Chlorite harzburgite Mg304 92-2 incs in olivine

Figure 6
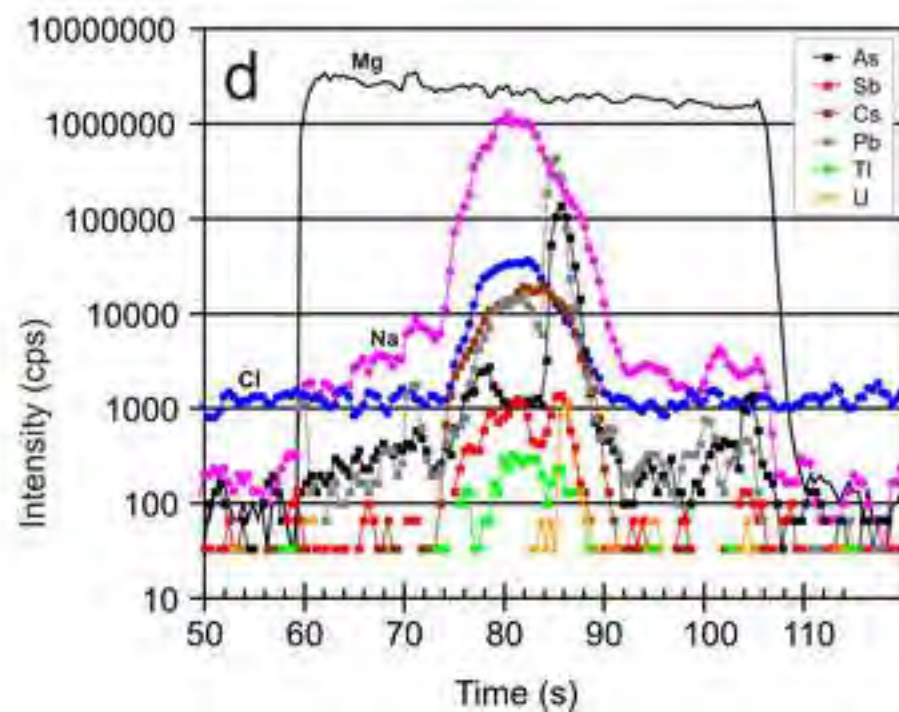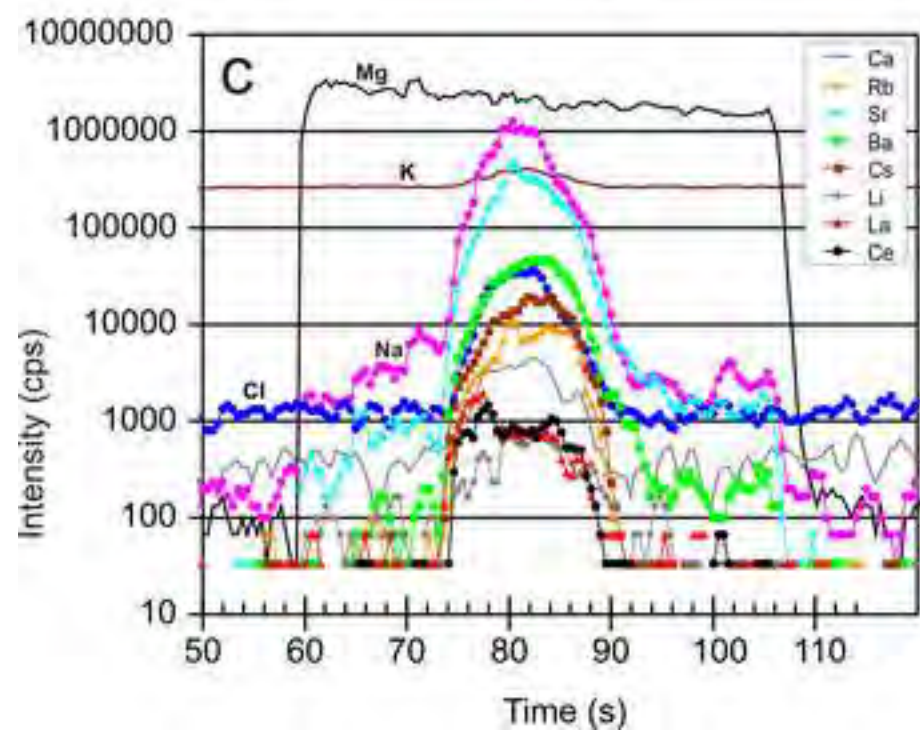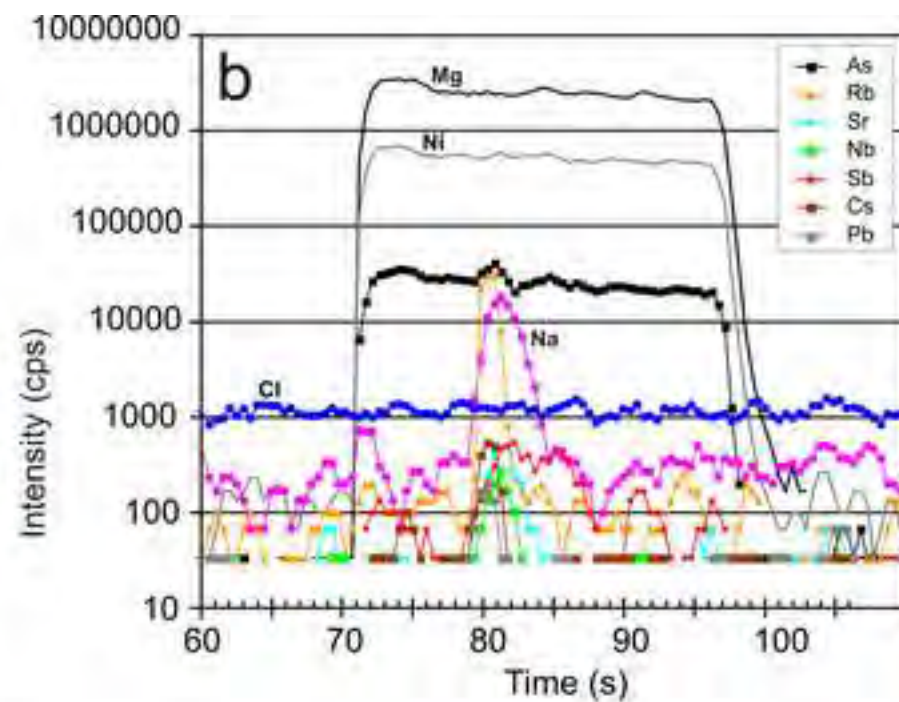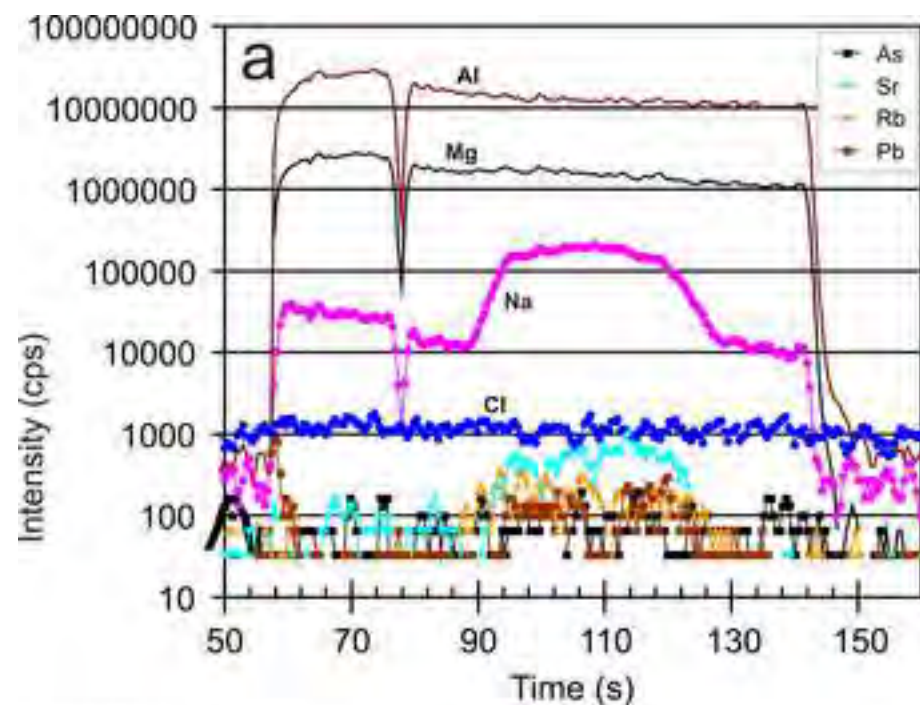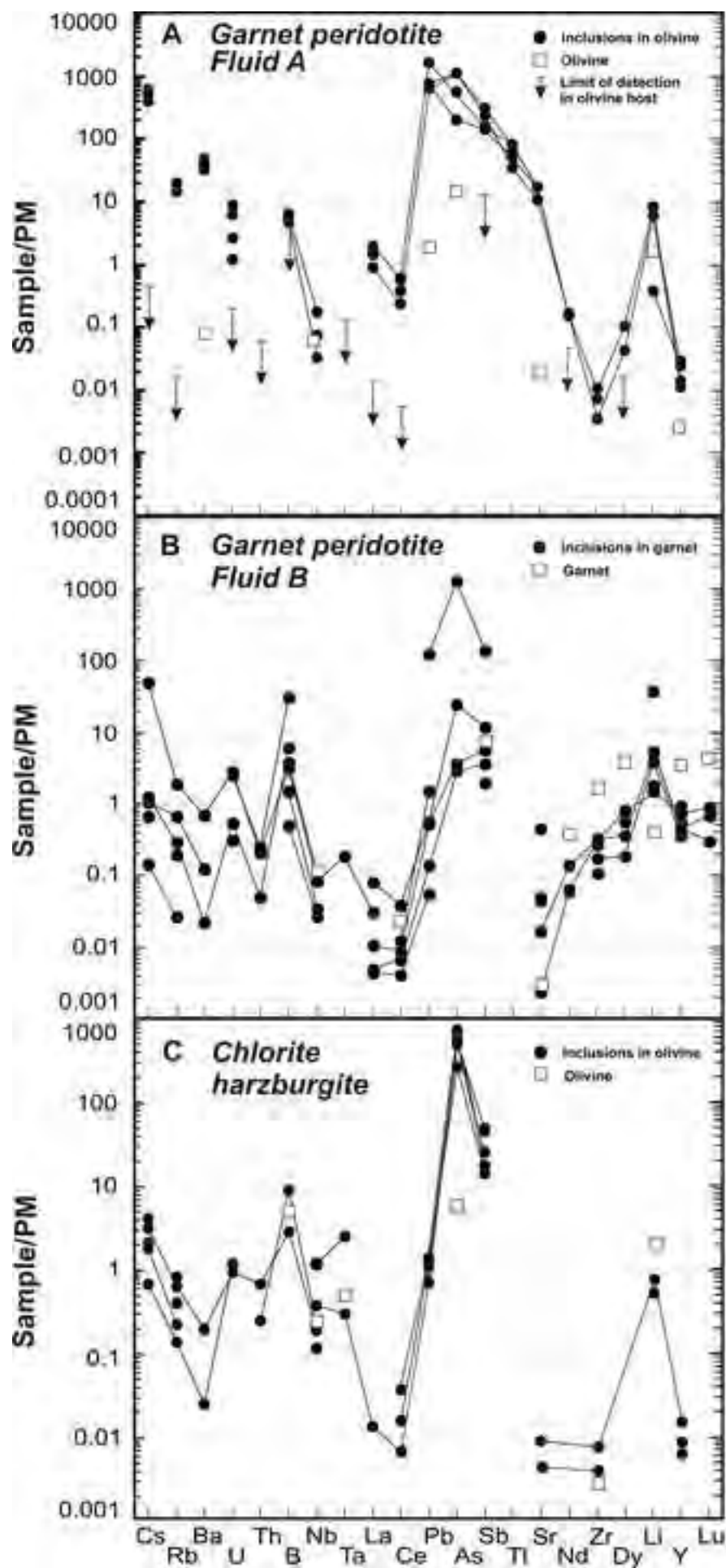[Click here to download high resolution image](#)

Figure 7
[Click here to download high resolution image](#)

Figure 8
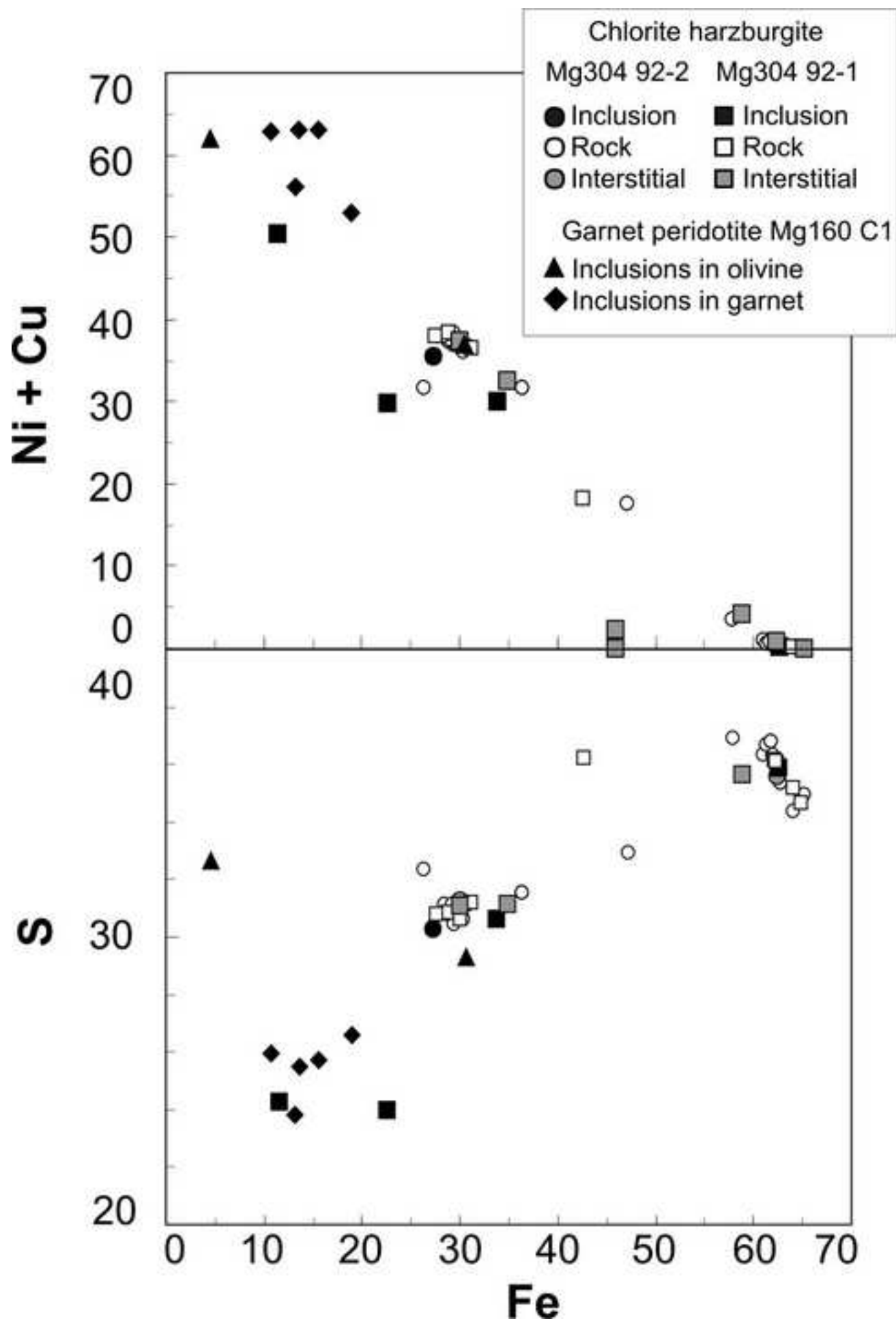Click here to download high resolution image

Figure 9
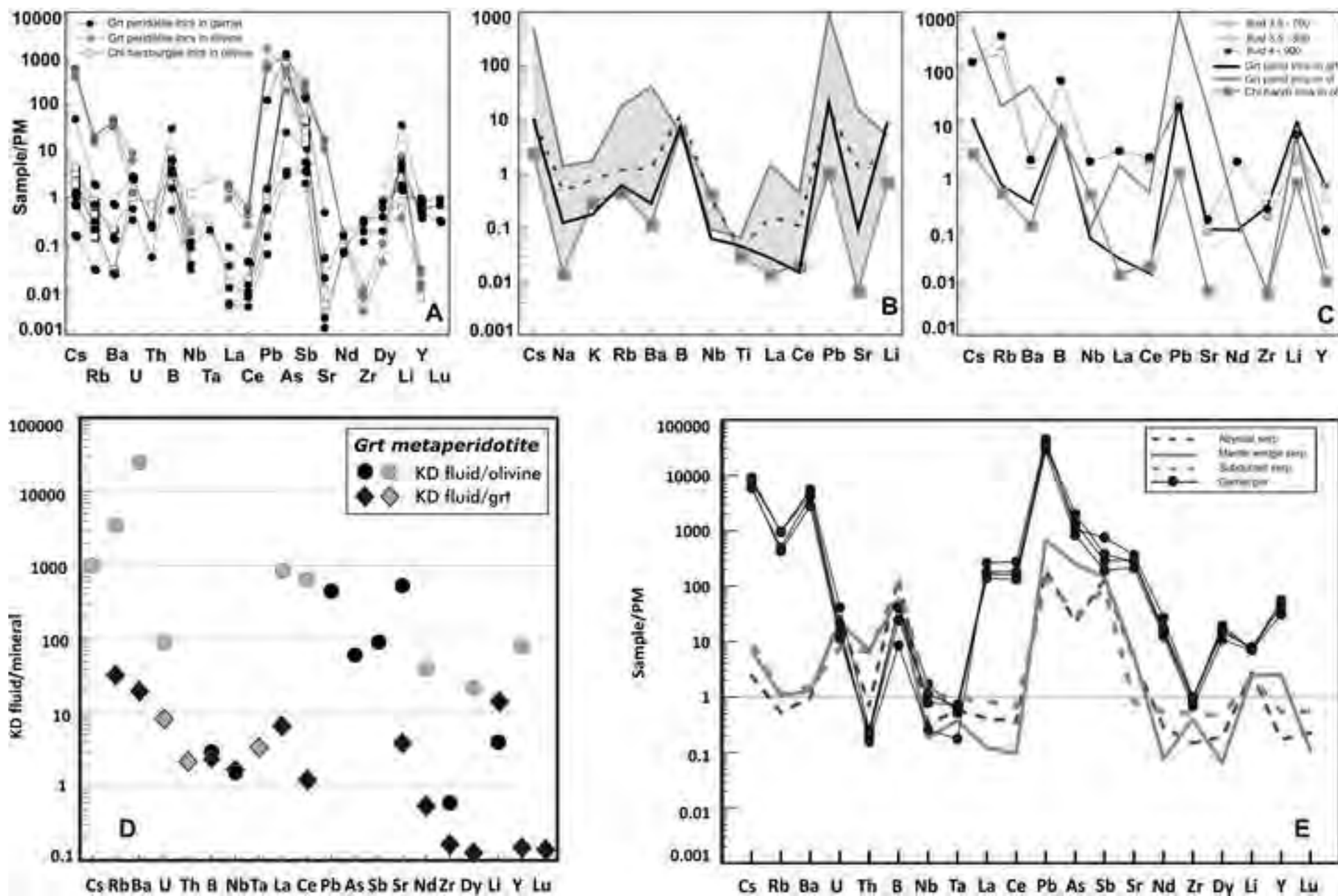**Click here to download high resolution image**

Table 1
Click here to download Table: Table 1.pdf

Table 1: LA-ICP-MS element concentration data for polyphase inclusions in garnet and olivine from Cima di Gagnone

		MG 160 C1; garnet host						MG 160 C1; olivine host					MG 304 92-2; olivine host				
Sample number		21frb04	21frb08	21frb09	21frb05	21frb06	21frb10	21frc08	21frc09	21frc11	21frc12	21frc13	21fra03	21fra11	21fra14	21fra15	21fra18
Inclusion size (µm)		40	40	55	40	55	58	25	40	22	22	18	22	60	25	25	26
	Mass																
SiO2	29	**10,00**	**10,00**	**9,00**	10,00	10,97	9,03	3,31	5,93	5,75	2,99	4,48	4,82	4,60	4,41	5,40	4,89
TiO2	49	0,0088	0,0041	0,0104	0,0105	0,0081	0,0129	0,0005	0,0124	0,0073	0,0013	0,0313	<0.0002	0,0017	0,0127	0,0089	0,0008
Al2O3	27	3,68	2,24	4,63	3,06	2,84	4,68	<0.0003	0,0033	<0.0006	0,0009	0,0010	0,0003	0,0025	0,0198	0,0012	0,0003
FeO	57	2,04	2,13	2,02	**0,17**	**0,17**	**0,17**	*<0.0004*	1,53	1,57	1,39	1,02	1,25	1,36	1,46	1,39	1,16
MgO	25	3,39	6,42	3,22	5,83	5,02	4,77	5,77	1,05	1,56	4,35	3,31	3,92	4,01	4,08	3,12	3,92
CaO	43	0,86	<0.01	1,10	0,74	0,80	1,24	0,47	0,91	0,56	0,72	0,62	<0.02	<0.008	<0.01	0,04	<0.03
Na2O	21	0,03	0,02	0,02	0,17	0,19	0,09	**0,50**	**0,50**	**0,50**	**0,50**	**0,50**	**0,01**	**0,01**	**0,01**	**0,01**	**0,01**
K2O	39	0,001	0,010	0,001	0,010	0,004	0,004	0,074	0,057	0,051	0,049	0,040	0,010	0,003	0,009	0,015	0,006
Sum		20,00	20,83	20,00	19,99	20,00	20,00	10,13	10,00	10,00	10,01	10,00	10,01	10,00	10,00	9,99	9,99
Li	7	2,9	*59*	2,4	8,6	6,4	8,5	9,3	11,8	0,6	8,8	12,1	<0.44	<0.10	<0.32	0,9	1,2
B	11	0,15	0,94	0,46	1,14	9,27	1,82	4,06	1,43	<1.50	1,95	1,84	2,69	<0.24	0,86	<1.62	<1.14
Cl	35	<22	800	40	<68	101	51	14100	17400	15500	14000	12600	155	43	114	<179	<131
Cr	53	2890	1080	2840	2620	236	2340	<7	96	<14	14	<13	<3	4	*394*	<4	<3
As	75	<0.02	*64*	0,1	<0.06	1,2	0,2	63	28	55	55	10	26	38	13	31	27
Rb	85	0,02	1,13	<0.005	0,41	0,12	0,18	8	12	9	11	12	0,25	0,08	0,39	0,50	0,14
Sr	88	0,03	*8,96*	0,05	0,91	0,99	0,34	170	350	220	330	340	<0.04	0,09	<0.03	0,18	<0.04
Y	89	2,40	4,11	3,19	1,96	1,58	1,94	0,08	0,11	0,09	0,06	0,04	0,039	0,027	0,066	<0.040	<0.037
Zr	90	2,77	<0.013	3,33	1,11	1,83	3,33	0,04	0,03	0,10	<0.03	0,07	<0.06	<0.01	0,04	0,08	<0.04
Nb	93	0,018	0,055	0,023	0,071	<0.009	<0.006	0,028	0,022	0,049	<0.02	0,114	0,149	0,255	0,125	0,792	0,077
Sb	121	0,01	0,14	0,02	<0.034	0,02	0,02	1,53	1,02	1,19	1,50	0,84	0,26	0,18	0,14	0,40	0,14
Cs	133	0,003	1,03	<0.002	0,022	0,014	0,027	4,9	12,7	8,3	11,6	10,8	0,045	0,014	0,068	0,087	0,038
Ba	137	<0.02	*4,6*	<0.02	0,8415	<0.04	0,149	128	320	220	290	270	<0.24	0,17	1,30	<0.32	<0.20
La	139	0,003	0,021	0,003	<0.006	0,053	0,007	0,33	1,25	0,59	1,05	0,94	<0.021	0,009	<0.020	<0.036	<0.028
Ce	140	0,007	<0.009	0,011	0,021	0,066	0,015	0,27	0,93	0,40	1,01	0,64	<0.025	0,011	0,027	0,063	<0.028
Nd	143	0,075	<0.06	0,083	<0.08	<0.04	0,176	<0.05	0,187	0,196	0,179	<0.14	<0.17	<0.05	<0.11	<0.13	<0.14
Dy	163	0,38	0,53	0,55	<0.02	0,12	0,24	0,044	0,026	<0.064	<0.056	0,064	<0.07	<0.01	<0.04	<0.10	<0.07
Lu	175	0,045	0,021	0,061	0,047	<0.002	0,020	n.a.	n.a.	n.a.	n.a.	n.a.	<0.016	<0.004	<0.010	<0.025	<0.015
Ta	181	<0.002	0,007	<0.001	<0.005	<0.002	<0.004	<0.007	<0.004	<0.017	<0.006	<0.016	<0.010	0,011	<0.013	0,092	<0.023
Tl	205	n.a.	n.a.	n.a.	n.a.	n.a.	n.a.	0,12	0,28	0,12	0,23	0,18	n.a.	n.a.	n.a.	n.a.	n.a.
Pb	208	0,009	*18,6*	0,021	0,225	0,086	0,078	61	240	95	110	112	0,16	0,11	0,19	0,21	0,11
Th	232	<0.001	0,017	<0.001	<0.002	0,020	0,004	0,004	<0.001	<0.024	<0.011	<0.015	0,020	<0.004	0,055	<0.034	<0.017
U	238	<0.002	0,064	0,007	<0.005	0,058	0,013	0,016	0,202	0,028	0,142	0,060	<0.021	0,028	0,022	<0.023	<0.017

Notes:

Element oxides are given in wt.%, elements in µg/g

Concentrations set in bold were used as the internal standard for data reduction (see text for explanations)

Entries "< value" represent limits of detection calculated for each element in every inclusion individually (Halter et al., 2002) employing the stringent LOD calculation from Pettke et al. (2012)

n.a. = not available

Values set in italic are deemed outliers and are not considered further

Note that the concentrations for Tl are to be taken with caution because Tl in SRM610 is heterogeneously distributed (Eggins and Shelley, 2002; Tl = 60 µg/g was used here)

Analytical Methods

Table R1

Table R2

Click here to download Supplementary material for online publication only: Table R2.xlsx

Table R3

Table R4